Electrical Power and Energy Systems 153 (2023) 109355

Contents lists available at ScienceDirect

International Journal of Electrical Power and Energy Systems

journal homepage: www.elsevier.com/locate/ijepes

Short-term uncertainty in the dispatch of energy resources for VPP: A novel rolling horizon model based on stochastic programming

F. Gulotta [a,*], P. Crespo del Granado [b], P. Pisciella [b], D. Siface [c], D. Falabretti [a]

[a] Davide Falabretti and Francesco Gulotta are with the Department of Energy, Politecnico di Milano, Milan, Italy
[b] Pedro Crespo del Granado and Paolo Pisciella are with the Department of Industrial Economics and Technology Management, Norwegian University of Science and Technology, Trondheim, Norway
[c] Dario Siface is with the Department of Energy System Development, Ricerca sul Sistema Energetico, Milan, Italy

ARTICLE INFO

Keywords:
Stochastic programming
Rolling horizon
Energy management system
Uncertainty
Virtual power plant

ABSTRACT

The intermittent nature of distributed energy resources introduces new degrees of uncertainty in the operation of energy systems; hence, short-term decisions can no longer be considered fully deterministic. In this article, an energy management system (EMS) was proposed to optimize the market participation and the real-time operation of a virtual power plant (VPP) composed of photovoltaic generators, non-flexible loads, and storage systems (e-vehicle, stationary battery, and thermal storage). The market bidding process was optimized through a two-stage stochastic formulation, which considered the day-ahead forecast uncertainty to minimize the energy cost and make available reserve margins in the ancillary service market. The real-time management of regulating resources was obtained through an innovative rolling horizon stochastic programming model, taking into account the effects of short-term uncertainties. Numerical simulations were carried out to demonstrate the effectiveness of the proposed EMS. The architecture proved to be effective in managing several distributed resources, enabling the provision of ancillary services to the power system. In particular, the model developed allowed an increase in the VPP's profits of up to 11% and a reduction in the energy imbalance of 25.1% compared to a deterministic optimization.

1. Introduction

The integration of distributed renewable energy sources (RESs) and the gradual electrification of end-uses are crucial factors in achieving environmental targets [1]. Upgrading the power system to reach these goals has proven to be a very challenging task; moreover, policies need to be deeply revised to facilitate RESs penetration and develop a smarter and more flexible grid, able to manage effectively the variability of Distributed Energy Resources (DERs).

In this regard, the aggregation of DERs in a virtual power plant (VPP) is an interesting option because it offers more predictable and controllable power outputs [2]. Moreover, by adopting suitable strategies, the VPP can also be controlled to provide ancillary services (e.g., frequency and balancing regulation) to the power system, increasing the number of flexibility providers and improving grid stability.

However, the stochastic nature of DERs introduces risks and uncertainties in all the decision-making phases of the VPP, namely, during the scheduling (i.e., market participation) and short-term decision phases (i.e., real-time operation). In the literature, there is consensus that the influence of these uncertainties must be taken into account in market participation that usually occurs from one day to some hours before the time of delivery [3,4]. The authors in [5] have investigated the influences of uncertainties during participation in the day-ahead market (DAM) by adopting a two-stage stochastic model. However, the effects of uncertainty on short-term decisions (i.e., real-time operation) have not been thoroughly analyzed, neither in [5] nor in the wider literature (see Section 2).

To address this limitation, this paper proposes a novel architecture capable of scheduling the resources available in a VPP (also applicable for aggregators) by considering the effects of the uncertainties in the short-term decision phase. The proposed architecture is composed of two layers.

The first layer has a two-stage stochastic model designed to define the optimal power schedule on the DAM and to offer reserve capacity on the ancillary service market (ASM). The second layer relies on an innovative rolling horizon stochastic programming model, which manages the controllable units in the VPP in real time in order to fulfill the

* Corresponding author.
E-mail address: francesco.gulotta@polimi.it (F. Gulotta).

https://doi.org/10.1016/j.ijepes.2023.109355
Received 28 December 2022; Received in revised form 7 June 2023; Accepted 30 June 2023
Available online 21 July 2023

Nomenclature

Acronyms

ARMA	Autoregressive Moving Average
AS	Ancillary Service
ASM	Ancillary Service Market
CS	Charging Station
D	Day of delivery
DAM	Day-Ahead Market
DER	Distributed Energy Resources
EMS	Energy Management System
ESS	Energy Storage System
EV	Electric Vehicle
MILP	Mixed-Integer Linear Programming
PDF	Probability Distribution Function
PV	PhotoVoltaic
RES	Renewable Energy Source
SoC	State of Charge
TSO	Transmission System Operator
VoPF	Value of Perfect Forecast
VoU	Value of Uncertainties
VPP	Virtual Power Plant

List of variables

$Cost^{S1/S2}$	first/second-stage cost
Imb	net power imbalance
Imb^{+}/Imb^{-}	positive/negative power imbalance
$P^{Abs,f}$	day-ahead power requirement forecast
P^{b}	water heater power absorption
$P^{b,nom}$	water heater nominal power
P^{buy}	power purchased on the DAM
$P^{X,FS}$	non-anticipativity auxiliary variable
$P^{ch,ESS}/P^{ds,ESS}$	charging/discharging ESS power
P^{EV}	EV power absorption
P^{DAM}	DAM power schedule
P^{sold}	power sold on the DAM
SoC^{ESS}	ESS SoC
SoC^{EV}	EV'SoC
T^{b}	internal temperature of the water heater
$z^{b,\min}/z^{b,Max}$	binary variables for the thermal comfort
z^{cap}	capacity remuneration binary variable
z^{sold}/z^{buy}	binary variable for purchased/sold DAM power
$z^{ch,ESS}/z^{ds,ESS}$	charging/discharging binary state of the ESS
z^{+}/z^{-}	imbalance sign binary variable
ΔP^{b}	water heater upward reserve margin
ΔP^{ESS}	ESS's upward reserve margin
ΔP^{EV}	EV's upward reserve margin
ΔP^{TOT}	overall upward reserve margin

List of parameters

c^{buy}/p^{buy}	cost/price per unit of purchase/sold energy
Cap	required reserved margin
C^{ESS}	energy capacity of the ESS
C^{EV}	energy capacity of the EV's battery
$\widetilde{h^{EV}}$	boolean parameter for EVs connection (uncertain)
M^{D}	upper bound for the power purchased/sold variable
M^{I}	upper bound for the power imbalance variable
M_{T}	upper bound for water temperature variable
P^{CS}	rated power of the charging station
P^{ESS}	maximum charging/discharging ESS power
$\widetilde{P^{PV}_{t,s}}/\widetilde{P^{L}_{t,s}}$	PV/load power profile forecast (uncertain)
p^{Cap}	daily revenue for the capacity reserved during the availability hours
$SoC^{EV,conf}$	desired EV's SoC
SoC^{min}/SoC^{Max}	upper/lower bound for the SoC
T^{0}	inlet water temperature
$T^{cnf,min}/T^{cnf,Max}$	upper/lower bounds of the comfort range
T^{env}	temperature of the air surrounding the water heater
$\widetilde{w^{cns}}$	expected hot water consumption (uncertain)
ΔT_{RH}	the length of the Rolling Horizon time window
$\Delta\widetilde{SoC^{usg}}$	expected EV's energy consumption (uncertain)
ϵ^{X}	ARMA-based forecast error
π_{s}	scenario probability of occurrence
η^{ch}/η^{ds}	ESS charging/discharging efficiency
$\eta^{EV,ch}$	EV's battery charging efficiency

List of indexes/Sets

n_{b}	water heater index ($\mathbb{N}^{B}$)
n_{e}	ESS index ($\mathbb{N}^{ESS}$)
n_{ev}	EV index ($\mathbb{N}^{EV}$)
s	index of scenarios analyzed ($\mathbb{S}^{DAM/RT}$)
t	time step index ($\mathbb{T}^{DAM}$)
t_{avb}	availability hours time step index ($\mathbb{T}^{avb}$)
t_{act}	time step in the delivery day ($\mathbb{T}^{D}$)

DAM commitment and provide ancillary services (AS) to the power system.

The proposed system was tested on a VPP composed of hundreds of residential users, equipped with rooftop photovoltaic (PV) plants, non-flexible loads, energy storage systems (ESSs), water heaters, and electric vehicles (EVs). The uncertainties of RES production, load consumption, and users' behavior (in terms of EV charging requests and hot water usage) were modeled in both layers by using real data. A central point of the analysis was to compare the rolling horizon stochastic programming model with its deterministic counterpart [6], to determine the value of considering the short-term uncertainty in real-time operations.

Following a literature review (Section 2), the framework of application and the mathematical models are described in Section 3. Then, Section 4 and Section 5 report the case study and the scenario generation procedure adopted to characterize the uncertainties affecting the problem, respectively. Section 6 and Section 7 present the numerical analyses carried out to assess the effectiveness of the proposed method. Finally, some conclusions are drawn.

2. Related works and main contributions to the state of the art

From the literature, several studies examined the market participation of aggregates of DERs and the architecture required to optimally manage their power exchanges in real time.

However, these two aspects have typically been investigated individually; hence, two separate research areas can be identified: *i*) strategies for bidding on the market and *ii*) strategies for the real-time control of resources. The first research area includes studies about optimization strategies to bid in the markets. The bidding strategy problem is examined from different perspectives in the literature. For the purposes of this study, the approaches adopted to model the uncertainties and resources included in the VPP were critically reviewed.

For example, the author in [7] proposed a two-stage stochastic problem to simulate the participation of the VPP in the DAM and spinning reserve market. The uncertainties that characterize RES and load

exchanges, energy prices, and flexibility activation were modeled by adopting a random sampling Monte Carlo method. However, errors affecting RES production were represented through univariate probability distribution functions (PDFs), neglecting the intercorrelation between forecast errors in succeeding time steps. Moreover, the VPP's real-time operation was not simulated by a dedicated tool. Hence, the resources were not re-scheduled according to the actual realization of the uncertain parameters. In [8], the bidding strategy of a VPP participating in the energy and reserve markets was studied. The authors developed a bi-level stochastic programming framework to define the VPP planning operation (upper level) and clear the energy and reserve markets (lower level). In particular, the VPP was modeled as a price-maker in both markets, allowing an increase in its expected profits. Furthermore, in this case, the real-time dispatch of the resources was not modeled.

Similarly, in [9], a model was proposed to optimize the day-ahead and reserve market participation of a VPP. Several uncertainties were considered, such as wind power production, flexibility activation, and market prices. The resulting stochastic optimization model was solved by adopting an iterative solution of a master problem and a subproblem. Despite the novelties of this study, the actual results achieved in real time were not tested. In [10], the authors proposed a mixed-integer linear programming (MILP) model to optimize the day-ahead and intra-day market participation; however, neither the real-time operation nor the uncertainties were modeled. In [11], a three-stage stochastic programming model was presented to optimize the offering process on the market. The uncertainties of the intermittent energy sources, customers' demand, and electricity prices were considered by generating several scenarios through autoregressive methods and PDFs. Finally, the fast-forward scenario reduction algorithm, developed by the authors in [12], was implemented to select representative scenarios. The real-time operation of the system was not simulated.

In [13], a bi-level stochastic optimization model was implemented to obtain the bidding strategy of a VPP in the day-ahead (first level) and balancing (second level) markets. The load and wind uncertainties were modeled considering random forecast errors with a zero mean, neglecting their time-dependent structure and not considering the real-time operation of the system.

In [14], a bi-level formulation was proposed to optimally declare the day-ahead and reserve market schedules for a VPP composed of conventional units, renewable resources, and interruptible loads. The model maximized the VPP's profit while minimizing the emissions of the units involved. However, neither the DAM uncertainties nor the impact of unexpected events during the real-time dispatch were modeled.

Similarly, the optimal bidding strategy of a VPP in joint day-ahead and reserve markets was studied in [15]. The day-ahead uncertainties were taken into account by considering stochastic scenarios, generated by shifting the deterministic forecast by constant values. The expected operation of the VPP on the following day was provided for the different scenarios; however, no dedicated tool was proposed to re-schedule the VPP units in real time, and short-term uncertainties were not considered.

The authors in [16] proposed robust optimization to manage the bidding strategy of a VPP in both the day-ahead and real-time markets. The uncertainties of wind production and market prices were implemented by an auto-regressive moving average (ARMA) model [17], capturing the temporal correlation of the forecast errors. In [18], the optimal day-ahead scheduling was obtained by maximizing the profit and minimizing the emissions of the VPP. The behavior of wind power, solar radiation and load, and the market prices were represented using a statistical approach based on univariate PDFs. Neither of these studies took the real-time operation of the system into account.

As is highlighted, most of the studies mainly focused on the VPP scheduling phase (e.g., by simulating its participation in electricity markets), without testing the actual performance achieved by the system during its operation (e.g., [7–11]).

The second research area identified in the literature, concerning the management of DER units in an aggregated form, includes studies proposing approaches to optimally control the VPP resources during real time.

In [19] and [20], real-time energy management systems were proposed to schedule a set of DERs and residential users. The optimal solution was achieved by solving distributed MILP problems, limiting the information shared with the central EMS. In these two papers, the effects of the systems' evolution in the upcoming time steps and the related uncertainties were not considered. Furthermore, the interactions between the VPP and the energy markets were not modeled.

In [21], the real-time optimal dispatch problem of a VPP composed by controllable generators, ESS, and flexible loads was studied. The VPP was managed as a multi-agent system and the real-time active power dispatch was obtained through the adoption of a distributed model predictive control. Hence, each resource was equipped with a control system that dispatched the power exchanges to pursue a local individual goal, also considering the information exchanged by the other units. Despite the VPP being mainly composed of unpredictable RES generation (wind and PV systems), the short-term uncertainties affecting the control horizon of the model predictive control were not considered. As in the previous case, the VPP participation in the market was neglected. In all of the studies found in the literature aiming at suggesting new approaches to the real-time dispatch of DER units, it became apparent that the interactions between the VPP and markets were not simulated. Furthermore, the effects of short-term uncertainties were always neglected.

To fill this gap in the literature, the architecture proposed in this paper was based on two different models that simulated both market participation and the real-time operation of the VPP. To the best of the authors' knowledge, this was the first paper to accurately model the effect of uncertainties in short-term decisions (i.e., during real-time dispatch).

Moreover, in several works (e.g., [7–10,13], and [18]), the uncertainties were represented as white noise phenomena, neglecting the time intercorrelation between errors in succeeding time steps. In the authors' opinion, this aspect is critical since the scenarios generated by this method are poorly diversified (i.e., they are distinguished by a zero-mean process), biasing the VPPs' decisions. Instead, in this work, the statistical characteristics of the uncertainties were preserved by adopting specifically designed autoregressive models.

Table 1 summarizes the main differences between the proposed approach (last row) and the studies analyzed, with the goal of highlighting the gap in the literature that this study aimed to fill.

Therefore, the main contributions of this article to the current state of the art were as follows:

- An integrated control architecture was proposed to effectively manage the market participation (DAM and ASM) and the real-time operation of a VPP including RES generation, non-controllable or partially controllable loads (EVs, water heaters), and ESSs. The reservation of a power band to supply ASs was also considered.
- A novel rolling horizon stochastic programming approach was designed to manage the operation phase (close to the real-time scheduling) of the system considering short-term uncertainties.
- A detailed model was implemented to simulate the power exchanges of residential water heaters. Furthermore, the thermal inertia of these flexible resources was exploited to make available a reserve margin and provide AS to the power system.
- An in-depth techno-economic assessment was performed to comprehensively evaluate the effects of uncertainties on the VPP's operation.
- Without losing any generality, a market framework coherent with the situation in place in many European countries was taken as a reference. Moreover, real-life data were considered concerning the activation requests of ASs, EV and load utilization, and RES energy exchanges.

Table 1
Comparison between the approaches available in the literature and this study.

Reference	Resources simulated	Market participation		Real-time dispatch		
		Simulated market platform	Optimization model adopted	Real-time dispatch	Optimization model adopted	Short-term uncertainty
[7]	DR, ESS, RES	DAM, SR	SP	×	×	×
[8]	CPP, ESS, RES	DAM, SM	SP bi-level optimization	×	×	×
[9]	CPP, DR ESS, RES	DAM, SR	ARSP	×	×	×
[11]	CPP, DR, ESS, RES	DAM, IM	SP (three-stage)	×	×	×
[13]	N-F Load, RES	DAM, BM	SP bi-level optimization	×	×	×
[14]	CPP, DR, ESS, RES	DAM, RTM	SP bi-level optimization	×	×	×
[16]	DR, ESS, RES	DAM, RTM	Two-stage robust	×	×	×
[19]	CPP, ESS, EV, RES	×	×	√	Multi-objective RT optimization	×
[20]	ESS, N-F Load, RES	×	×	√	Distributed MILP optimization	×
[21]	CPP, ESS, N-F Load, RES	×	×	√	DMPC	×
This work	**ESS, EV, N-F load, WH, RES**	**DAM, BM**	**SP**	√	**Rolling Horizon SP**	√

CPP: conventional power plant, DR: demand response, N-F load: non-flexible load, WH: water heater.
BM: balancing market, ID: intra-day market, RTM: real-time market, SP: spinning reserve.
ARSP: adaptive robust stochastic programming, DMPC: distributed model predictive control, MILP: mixed-integer linear programming, RT: real time, SP: stochastic programming.

3. Problem description and formulation

The control strategy proposed aimed to optimize the DAM and ASM participation and management in the real-time operation of a VPP composed of: *i*) PV panels, *ii*) non-flexible residential loads, *iii*) water heaters, *iv*) charging stations for EVs, and *v*) ESSs.

The VPP operates as follows:

a) On day D-1, a binding power curve is declared on the DAM to supply the local load and sell the PV power production. The VPP makes decisions on the power traded on the DAM based on the available forecasts and corresponding uncertainties. Moreover, the amount of frequency restoration and replacement reserves [22] to be offered on the ASM for specific hours of day D (hereafter referred to as availability hours) is defined. According to the discipline currently in place in Italy for VPP projects [23], an amount of upward reserve at least equal to a predetermined threshold (*Cap*) must always be guaranteed by the VPP to the transmission system operator (TSO).
b) On day D, during the availability hours, the TSO can activate the reserved flexibility to solve grid criticalities.
c) In real time, the VPP dispatches the available flexible resources (i.e., ESSs, EVs, and water heater), to: *i*) respect the DAM market commitment and minimize the power mismatches and the corresponding fees (i.e., imbalance cost) [22], *ii*) ensure upward reserve capacity during the availability hours, *iii*) provide the requested AS,

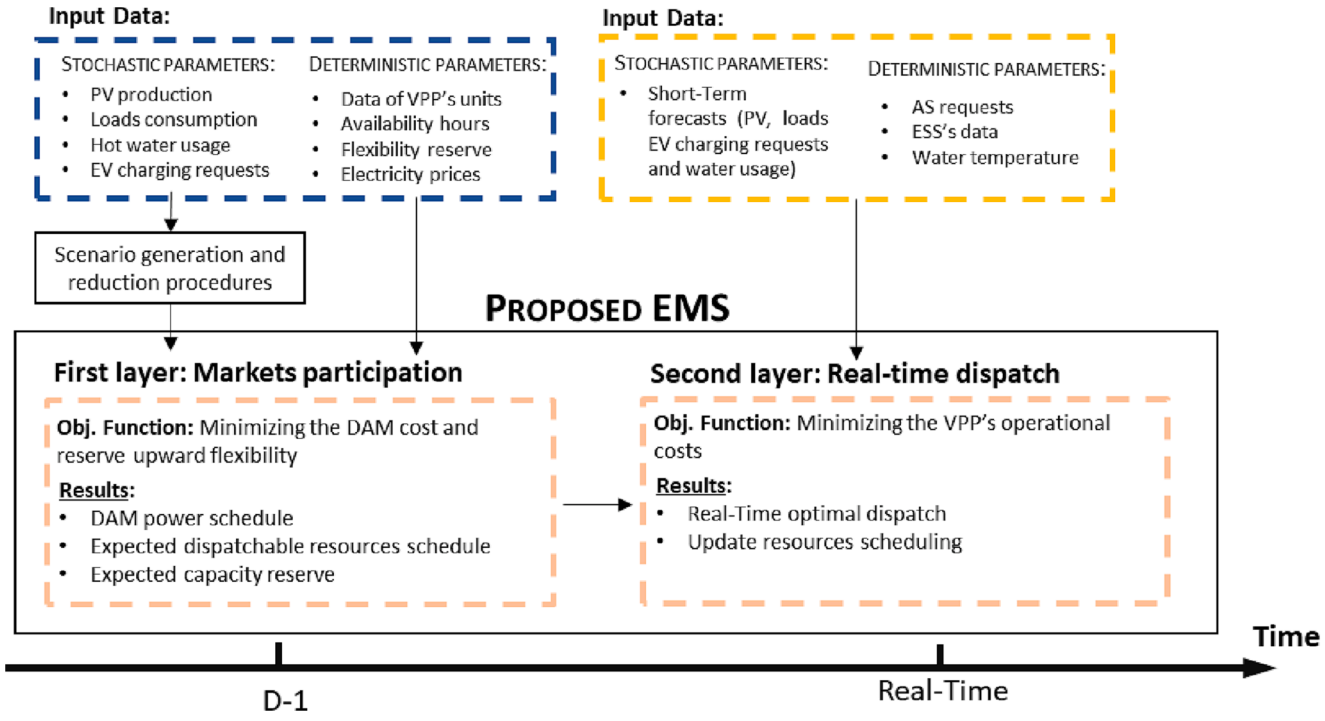

Fig. 1. Schematic representation of the EMS.

and *iv*) maintain an adequate level of comfort for residential users, both in terms of EV charging profiles and hot water temperature.

The schematic description of the EMS is presented in Fig. 1. The first layer, executed on day D-1, is devoted to optimally defining the DAM power schedule and offering the available regulation reserve on the ASM. As is shown, different stochastic and deterministic parameters are used as inputs of the proposed two-stage stochastic model. Before solving the optimization problem, the day-ahead uncertainties are modeled using a scenario generation procedure. Then, in each time step of the delivery day (D), the rolling horizon stochastic programming model (i.e., second layer) is executed. It dispatches, in real time, the regulation resources considering the evolution of the uncertainties in the next future.

3.1. Market participation

The day before the day of delivery (day D-1), the expected power exchange of the VPP was required to be declared on the market to buy (or sell) the energy required (or produced) by all the users involved in the system. Furthermore, the VPP could offer its upward reserve on the ASM. For this purpose, an optimized power schedule for the VPP was necessary:

- to minimize the DAM cost (e.g., exploiting self-consumption and energy arbitrage);
- to mitigate forecast errors (i.e., minimize imbalance fees);
- to guarantee a reserve margin to supply regulation services in case of AS request.

The day-ahead forecast of the energy requirement is subject to strong uncertainties [24], which must be adequately considered in the optimization process. To handle these uncertainties, stochastic programming and robust optimization are generally considered as alternative choices. In the former, it is assumed that the probability distribution functions of the uncertain parameters are known. Instead, the latter seeks to find a solution that is optimal for the worst case within a given uncertainty set. Therefore, robust optimization is generally adopted for problems with constraints that must be respected despite the realization of the uncertainties (i.e., no latitude for violation is accepted). On the other hand, in stochastic programming, the decision variables are defined to optimize the expected outcomes of uncertain parameters. An exhaustive comparison between stochastic programming and robust optimization methods was provided in [2]. In this work, a two-stage stochastic programming model was adopted.

In stochastic programming, random variables are usually represented by a finite set of realizations, called scenarios. Hence, each scenario is characterized by a different forecast of uncertain parameters and probability of occurrence [25].

In a two-stage stochastic optimization, two classes of variables are defined [26]. The first-stage variables represent decisions made before knowing the realization of the uncertainties. Thus, first-stage variables represent a decision that must be made based on the available information, without the knowledge of future events. For this reason, first-stage variables are also called *here-and-now* variables. On the other hand, second-stage variables are made after knowing the actual realization of the aleatory parameters. Hence, these decisions depend on the uncertainty realization and they model corrective actions taken to compensate for any undesirable outcomes. Usually, stochastic models are solved considering the expected cost, calculated as the sum between the first-stage cost (i.e., cost experienced before the uncertainty realization) and the weighted sum of the second-stage costs (i.e., cost incurred after the realization of uncertain parameters). The weights correspond to the probability of occurrence of each scenario and the sum of probabilities over all scenarios is equal to 1. However, risk-based measurements, such as the conditional value at risk, can also be included in the objective function [26].

In this model, the first-stage variables referred to the power declared on the DAM and the capacity reserve offered on the ASM, since all these decisions were made one day in advance, before knowing the actual realization of the uncertainty parameters. On the other hand, the second-stage variables describe the decisions set after the result of uncertainties is revealed and thus represent the expected operation for day D. It is worth noting that the expected operation forecasted on day D-1 by the first layer of the EMS differed from the actual dispatch adopted in real time (achieved by the second layer). This is because, in general, the uncertain parameters forecasted during the market participation do not coincide with the actual realization in real time.

The DAM power schedule (first-stage variable), hereafter P_t^{DAM}, is indexed by t, where $t \in \mathbb{T}^{DAM}$ indicates the time steps of day D. In each time step, the VPP can either inject ($P_t^{DAM} < 0$) or absorb ($P_t^{DAM} > 0$) power from the grid. Hence, the following constraints are introduced:

$$P_t^{DAM} = P_t^{buy} - P_t^{sold} \tag{1}$$

$$0 \le P_t^{buy} \le M^D Z_t^{buy} \tag{2}$$

$$0 \le P_t^{sold} \le M^D Z_t^{sold} \tag{3}$$

$$z_t^{sold} + z_t^{buy} \le 1 \tag{4}$$

Constraints (2)–(4) avoid the simultaneous injection and withdrawal of power. Moreover, Eq. (1) evaluates the costs/revenues for the energy purchased ($P_t^{DAM} > 0$) and sold ($P_t^{DAM} < 0$). The parameter M^D is a positive upper bound for P_t^{buy} and P_t^{sold}, while z_t^{sold} and z_t^{buy} are two mutually exclusive binary variables.

The second-stage problem modeled the expected operation of the system on day D in different scenarios indexed by s, where $s \in \mathbb{S}^{DAM}$. Each scenario simulated a different realization of the uncertainty. In this study, the uncertain parameters were indexed by t and s (e.g., $\widetilde{l_{t,s}}$) to underline both the time and scenario dependency, and they were labeled with a tilde.

To optimally bid on the markets, the first layer of the EMS considered the expected usage of the dispatchable resources (i.e., ESSs, EVs, and water heaters) on the following day. This allows for exploitation of the regulating capabilities of these resources to minimize the DAM costs and allows the reserve margin on the ASM to be offered. In this regard, two classes of variables were employed. Variables denoted as P_t^X represent the power exchanged by the flexible resources X, while variables indicated as ΔP^X represent the reserve margin that the flexible asset X can make available, i.e., the ΔP^X variables denote the power capacity retained by the EMS to be able to supply the service when it will be requested by the TSO.

Each ESS, indicated by $n_e \in \mathbb{N}^{ESS}$, is modeled by the following equations:

$$SoC_{t,s,n_e}^{ESS} = SoC_{t-1,s,n_e}^{ESS} + \frac{\left(P_{t,s,n_e}^{ch,ESS}\eta^{ch} - P_{t,s,n_e}^{ds,ESS} \Big/ \eta^{ds}\right)}{C_{n_e}^{ESS}} \tag{5}$$

$$SoC^{min} \le SoC_{t,s,n_e}^{ESS} \le SoC^{Max} \tag{6}$$

$$z_{t,s,n_e}^{ch,ESS} + z_{t,s,n_e}^{ds,ESS} \le 1 \tag{7}$$

$$0 \le P_{t,s,n_e}^{ch,ESS} \le P_{n_e}^{ESS} z_{t,s,n_e}^{ch,ESS} \tag{8}$$

$$0 \le P_{t,s,n_e}^{ds,ESS} \le P_{n_e}^{ESS} z_{t,s,n_e}^{ds,ESS} \tag{9}$$

$$P_{t,s}^{ESS,abs} = \sum_{n_e \in \mathbb{N}^{ESS}} P_{t,s,n_e}^{ch,ESS} - P_{t,s,n_e}^{ds,ESS} \tag{10}$$

Eq. (5) represents the energy balance of the ESS, where SoC^{ESS} is the

state of charge of the ESS, $P^{ch,ESS}_{t,s,n_e}/P^{ds,ESS}_{t,s,n_e}$ are the expected charging/discharging power of the battery, and $C^{ESS}_{n_e}$ is its energy capacity. Constant charging and discharging efficiencies were considered (η^{ch} and η^{ds}, respectively), since the development of a detailed model of the battery was beyond the scope of this study. The SoC in Eq. (6) is bounded between its minimum and maximum values [27]. Simultaneous charge and discharge is avoided by constraints (7)–(9), where $z^{ch,ESS}_{t,s,n_e}$ and $z^{ds,ESS}_{t,s,n_e}$ are two mutually exclusive binary variables. Eq. (10) evaluates the total power exchanged by the batteries ($P^{ESS,abs}_{t,s}$).

The second-stage problem must also consider the requirement to reserve flexibility margin during the availability hours t_{avb}, where $t_{avb} \in \mathbb{T}^{avb}$. The ESS's upward reserve ($\Delta P^{ESS}_{t_{avb},s,n_e}$) is calculated as the maximum allowed power variation with respect to the expected net power absorption (i.e., $P^{ch,ESS}_{t_{avb},s,n_e} - P^{ds,ESS}_{t_{avb},s,n_e}$).

$$-P^{ESS}_{n_e} \le \Delta P^{ESS}_{t_{avb},s,n_e} + \left(P^{ch,ESS}_{t_{avb},s,n_e} - P^{ds,ESS}_{t_{avb},s,n_e}\right) \le +P^{ESS}_{n_e} \tag{11}$$

$$\Delta SoC^{ESS}_{t_{avb},s,n_e} = \frac{\Delta P^{ESS}_{t_{avb},s,n_e}}{C^{ESS}_{n_e}} \tag{12}$$

$$SoC^{min} \le SoC^{ESS}_{t_{avb},s,n_e} + \Delta SoC^{ESS}_{t_{avb},s,n_e} \le SoC^{Max} \tag{13}$$

$$\Delta P^{ESS,TOT}_{t_{avb},s} = \sum_{n_e \in \mathbb{N}^{ESS}} \Delta P^{ESS}_{t_{avb},s,n_e} \tag{14}$$

$\Delta P^{ESS}_{t_{avb},s,n_e}$ represents the maximum upward reserve that each ESS can make available and it is constrained by the maximum charging/discharging power in Eq. (11) and the battery's SoC in Eq. (12) and (13).

Fig. 2 exemplifies the effects of the constraints introduced. For example, if an ESS is discharging at time t (see the blue marker in Fig. 2), the green area would represent the maximum available upward reserve considering only the power limits (Eq. (11) alone), i.e. the available power margin to reach the full discharge power. However, since ESSs are energy-limited devices, their energy content must also be checked (see yellow area). This is carried out by including in the problem the constraint in Eq. (13), which evaluates the reserve considering also the energy limits.

The overall flexibility margin of the ESSs ($\Delta P^{ESS,TOT}_{t_{avb},s}$) is calculated using Eq. (14). In the proposed formulation, two peculiar aspects must be noticed: *i*) Eq. (11)–(14) are applied only during the availability hours (i.e., $\forall t_{avb} \in \mathbb{T}^{avb}$) and *ii*) $\Delta P^{ESS}_{t_{avb},s,n_e}$ models the available reserve margin of the ESS and it does not represent a real variation in the power exchanged, which is $P^{ch,ESS}_{t_{avb},s,n_e} - P^{ds,ESS}_{t_{avb},s,n_e}$.

Concerning electric mobility, each EV is indicated by the index $n_{ev} \in \mathbb{N}^{EV}$. In this study, both the instant of connection of the EV to the charging station (CS) and its initial SoC are considered uncertain. The former is modeled by the Boolean parameter $\widetilde{h^{EV}_{t,s,n_{ev}}}$, equal to 1 if the n_{ev}-th vehicle of scenario s is connected to the CS at time step t, and zero otherwise. The initial SoC depends on $\Delta\widetilde{SoC^{usg}_{t,s,n_{ev}}}$, which represents the forecasted energy consumption of the EV during the utilization by the owner. To model the EVs' behavior, the following equations are used:

$$SoC^{EV}_{t,s,n_{ev}} = -\Delta\widetilde{SoC^{usg}_{t,s,n_{ev}}} + SoC^{EV}_{t-1,s,n_{ev}} + \frac{\left(P^{EV}_{t,s,n_{ev}}\eta^{EV,ch}\right)}{C^{EV}_{n_{ev}}} \tag{15}$$

$$SoC^{min} \le SoC^{EV}_{t,s,n_{ev}} \le SoC^{Max} \tag{16}$$

$$0 \le P^{EV}_{t,s,n_{ev}} \le P^{CS}_{n_{ev}} \widetilde{h^{EV}_{t,s,n_{ev}}} \tag{17}$$

$$P^{EV,abs}_{t,s} = \sum_{n_{ev} \in \mathbb{N}^{EV}} P^{EV}_{t,s,n_{ev}} \tag{18}$$

Eq. (15) models the EV's battery SoC ($SoC^{EV}_{t,s,n_{ev}}$), which is bounded in a feasible range by Eq. (16). $\eta^{EV,ch}$ and $C^{EV}_{n_{ev}}$ represent the overall charging efficiency and the EV's battery capacity, respectively, while $P^{EV}_{t,s,n_{ev}}$ is the power absorption of each EV. The EMS can manage only the power absorption of EVs connected to a CS (i.e., when $\widetilde{h^{EV}_{t,s,n_{ev}}} = 1$); therefore, Eq. (17) imposes $P^{EV}_{t,s,n_{ev}} = 0$ when the EV is not connected ($\widetilde{h^{EV}_{t,s,n_{ev}}} = 0$) and $0 \le P^{EV}_{t,s,n_{ev}} \le P^{CS}_{n_{ev}}$ otherwise, where $P^{CS}_{n_{ev}}$ is the CS rated power. Eq. (18) calculates the total power absorbed by the EVs ($P^{EV,abs}_{t,s}$).

Fig. 3 exemplifies the formulation proposed. In the example, a scenario s is considered in which the EV is expected to be outside of the home location between 8 am and 4 pm. In this period, $\widetilde{h^{EV}_{t,s,n_{ev}}} = 0$; thus, the charging power $P^{EV}_{t,s,n_{ev}}$ is set to 0 and $\Delta\widetilde{SoC^{EV}_{t,s,n_{ev}}}$ is greater than zero, modeling the estimated energy consumption of the car during its use. Instead, when the EV is connected to the CS, $\widetilde{h^{EV}_{t,s,n_{ev}}} = 1$; therefore, the power absorption from the grid can be modulated between 0 and $P^{CS}_{n_{ev}}$ (green area).

The DAM schedule should ensure the charging of all EVs prior to departure. For this purpose, constraint (19) restricts the domain to solutions that guarantee that, when the EV leaves the CS (i.e., $t = t_{dep}$), the SoC is higher that a minimum acceptable threshold ($SoC^{EV,conf}$).

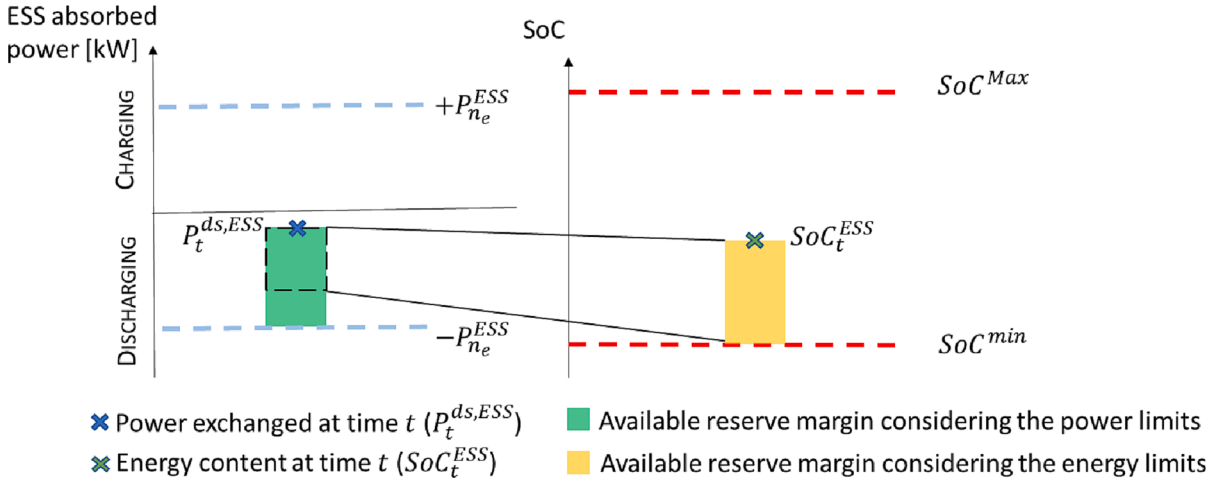

Fig. 2. Example of the admissible upward reserve margin considering only the power limits (green area) and the energy limits (in yellow). The dotted line represents the projection of the yellow area into the power domain. In this example, the available power reserve is limited by the energy level.

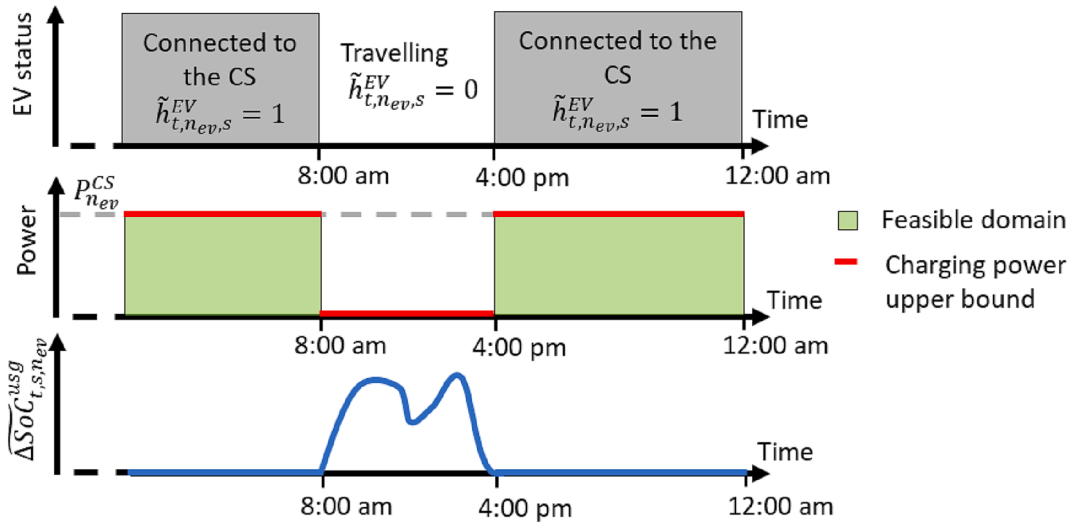

Fig. 3. Approach proposed to constrain the admissible EV charging power domain.

$$SoC^{EV}_{t,s,n_{ev}} \geq SoC^{EV,conf} \;\; if \;\; t = t_{dep} \tag{19}$$

EVs are considered partially dispatchable resources. Their reserve margin during the availability hours (t_{avb}) is evaluated through the following equations:

$$0 \leq \Delta P^{EV}_{t_{avb},s,n_{ev}} + P^{EV}_{t_{avb},s,n_{ev}} \leq P^{CS}_{n_{ev}} \widetilde{h^{EV,con}_{t_{avb},s,n_{ev}}} \tag{20}$$

$$\Delta SoC^{EV}_{t_{avb},s,n_{ev}} = \frac{\Delta P^{EV}_{t_{avb},s,n_{ev}}}{C^{EV}_{n_{ev}}} \tag{21}$$

$$SoC^{min} \leq SoC^{EV}_{t_{avb},s,n_{ev}} + \Delta SoC^{EV}_{t_{avb},s,n_{ev}} \leq SoC^{Max} \tag{22}$$

$$\Delta P^{EV,TOT}_{t_{avb},s} = \sum_{n_{ev} \in \mathbb{N}^{EV}} \Delta P^{EV}_{t_{avb},s,n_{ev}} \tag{23}$$

Also in this case, the EV's available reserve margin ($\Delta P^{EV}_{t_{avb},s,n_{ev}}$) is limited both in terms of maximum power (Eq. (20)) and battery energy content (Eq. (21) and (22)). Parameter $\widetilde{h^{EV}_{t_{avb},s,n_{ev}}}$ in Eq. (20) allows modulation of the charging power of vehicles connected to a CS.

The expected power withdrawal of each water heater is forecasted, on day D-1, to reserve an upward capacity margin and minimize the DAM cost (e.g., by maximizing the self-consumed energy). To model each water heater $n_b \in \mathbb{N}^B$, the following equations are adopted:

$$T^b_{t,s,n_b} = T^b_{t-1,s,n_b} - \frac{T^b_{t,s,n_b} - T^{env}}{RS_W V_{n_b} \rho} - \frac{\widetilde{w^{cns}_{t,s,n_b}} \left(T^b_{t,s,n_b} - T^0\right)}{V_{n_b}} + \frac{P^b_{t,s,n_b}}{S_W V_{n_b} \rho} \tag{24}$$

$$0 \leq P^b_{t,s,n_b} \leq P^{b,nom}_{n_b} \tag{25}$$

$$T^0 \leq T^b_{t,s,n_b} \leq T^{MAX} \tag{26}$$

$$P^{b,abs}_{t,s} = \sum_{n_b \in \mathbb{N}^B} P^b_{t,s,n_b} \tag{27}$$

The water heater's temperature (T^b_{t,s,n_b}) is described by the energy balance in Eq. (24), derived from [28]. The formulation takes into consideration: the temperature in the previous time step (T^b_{t-1,s,n_b}), the heat dispersions (second term of (24)), the temperature reduction for the expected use of water ($\widetilde{w^{cns}_{t,s,n_b}}$), and the temperature increase obtained by the electric power absorption (P^b_{t,s,n_b}). The water usage strongly affects the water heater's power request; therefore, the uncertainties that influence $\widetilde{w^{cns}_{t,s,n_b}}$ are also considered. Eq. (25) bounds the heater power (P^b_{t,s,n_b}) between zero and its nominal power ($P^{b,nom}_{n_b}$). Infeasible solutions are avoided by constraint (26), which ensures that the value of water temperature will remain between the inlet (T^0) and maximum (T^{MAX}) limits. If temperature goes outside the comfort range, the VPP manager must refund the users. To model this aspect, a Big-M formulation is adopted [29].

$$T^{cnf,Max} - T^b_{t,s,n_b} \geq -M_T z^{b,Max}_{t,s,n_b} \tag{28}$$

$$T^b_{t,s,n_b} - T^{cnf,min} \geq -M_T z^{b,min}_{t,s,n_b} \tag{29}$$

$$z^{b,min}_{t,s,n_b} + z^{b,Max}_{t,s,n_b} \leq 1 \tag{30}$$

Parameters $T^{cnf,Max}$ and $T^{cnf,min}$ are the upper and lower bounds of the comfort range, respectively. If the water heater temperature (T^b_{t,s,n_b}) is inside the limits ($[T^{cnf,min}; T^{cnf,Max}]$), Eq. (28) and (29) hold if, and only if, the two binary variables, $z^{b,Max}_{t,s,n_b}$ and $z^{b,min}_{t,s,n_b}$, are zero. Instead, if the water temperature is too high ($T^b_{t,s,n_b} > T^{cnf,Max}$) or too low ($T^b_{t,s,n_b} < T^{cnf,min}$), Eq. (28) or (29) are alternately satisfied if $z^{b,Max}_{t,s,n_b} = 1$ or $z^{b,min}_{t,s,n_b} = 1$. These two binary variables are adopted in the objective function to evaluate the fees that the VPP owner owes the users in the case of non-fulfillment of thermal comfort.

Also, the thermal inertia of the water heaters is exploited by the EMS to supply a reserve margin to the power system ($\Delta P^b_{t_{avb},s,n_b}$). To ensure the feasibility of the solution, the following equations are adopted:

$$0 \leq P^b_{t_{avb},s,n_b} + \Delta P^b_{t_{avb},s,n_b} \leq P^{n,nom}_{n_b} \tag{31}$$

$$\Delta T^b_{t_{avb},s,n_b} = \frac{\Delta P^b_{t_{avb},s,n_b}}{S_W V_{n_b} \rho} \tag{32}$$

$$T^0 \leq T^b_{t_{avb},s,n_b} + \Delta T^b_{t_{avb},s,n_b} \leq T^{MAX} \tag{33}$$

$$\Delta P^{b,TOT}_{t_{avb},s} = \sum_{n_b \in \mathbb{N}^B} \Delta P^b_{t_{avb},s,n_b} \tag{34}$$

The heater upward reserve is limited in a feasible domain by Eq. (31)–(33), while the total reserved margin obtained by all water heaters in the VPP ($\Delta P^{b,TOT}_{t_{avb},s,n_b}$) is calculated through Eq. (34).

On the delivery day D, the VPP is subject to economic penalties, so-called imbalance fees, in case of mismatches between the power schedule on the DAM (P^{DAM}_t) and the actually exchanged one ($P^{Abs,f}_{t,s}$) [30], as defined in Eq. (35). The amount of imbalance is known only a

posteriori, after the actual occurrence of the events. However, during the DAM participation, the perspective imbalance obtained in the different stochastic scenarios ($P^{Abs,f}_{t,s}$) is calculated considering the contributions of the flexible resources (ESSs, EVs, and water heaters), PV plants ($\widetilde{P^{PV}_{t,s}}$), and non-flexible loads ($\widetilde{P^{L}_{t,s}}$), as shown in Eq. (36). Eq. (37)–(40) allow the separation of positive ($Imb^{+}_{t,s}$) and negative ($Imb^{-}_{t,s}$) imbalances, since they are priced differently. Moreover, the proposed formulation prevents the contemporary presence of imbalances in both directions, which is infeasible.

$$Imb_{t,s} = P^{DAM}_{t} - P^{Abs,f}_{t,s} \tag{35}$$

$$P^{Abs,f}_{t,s} = P^{ESS,abs}_{t,s} + P^{EV,abs}_{t,s} + P^{b,abs}_{t,s} - \widetilde{P^{PV}_{t,s}} + \widetilde{P^{L}_{t,s}} \tag{36}$$

$$Imb_{t,s} = Imb^{+}_{t,s} - Imb^{-}_{t,s} \tag{37}$$

$$0 \le Imb^{+}_{t,s} \le M^{I} z^{+}_{t,s} \tag{38}$$

$$0 \le Imb^{-}_{t,s} \le M^{I} z^{-}_{t,s} \tag{39}$$

$$z^{+}_{t,s} + z^{-}_{t,s} \le 1 \tag{40}$$

The VPP owner could offer the upward regulating capacity during availability hours on the ASM. In this work, the VPP is supposed to be paid with a dual remuneration scheme similar to the one currently in place in Italy [23], in which both the availability to supply upward power regulation and the actual energy activated during the service provision are rewarded (payments proportional to the reserve margin available and the energy exchanged for the ASs supply, respectively). This is implemented by adopting the following equations:

$$\Delta P^{TOT}_{t_{avb},s} = \Delta P^{ESS,TOT}_{t_{avb},s} + \Delta P^{EV,TOT}_{t_{avb},s} + \Delta P^{b,TOT}_{t_{avb},s} \tag{41}$$

$$-\Delta P^{TOT}_{t_{avb},s} \ge z^{cap} Cap \tag{42}$$

where Eq. (41) evaluates the overall upward reserve margin available ($\Delta P^{TOT}_{t_{avb},s} \le 0$) and Eq. (42) ensures that the binary variable z^{cap} is set to 1 if the VPP is able to offer on the ASM a quota of the reserve greater than the one required by the TSO (Cap). It is worth noting that the binary variable z^{cap} is a first-stage variable (it is not indexed by s), since the ASM session precedes real time (when the uncertainty realizations are known). The binary variable z^{cap} is included in the objective function to assess the reserve availability payment. Hence, the EMS schedules the power exchanges by regulating resources (i.e., $P^{ESS,abs}_{t,s}$, $P^{EV,abs}_{t,s}$, and $P^{b,abs}_{t,s}$) also to guarantee the availability of a quota of reserve sufficiently high to receive the reserve availability payment.

In the proposed formulation, the DAM power curve (P^{DAM}_{t}) and the reserve capacity are obtained by minimizing the expected costs, calculated as a weighted sum of the first-stage and second-stage costs (Eq. (43)), where the weights π_s correspond to the scenario occurrence probabilities.

First-stage costs in Eq. (44) are related to the economic flows occurring before real time, such as the expected revenues (Rev^{Cap}) obtained for having made available an amount of regulation reserve at least equal to Cap and the costs/revenues for the energy acquired/sold on the DAM ($Cost^{DAM}_{t}$). In Eq. (44), c^{buy}_{t} and p^{buy}_{t} are the cost/price per unit of purchase/sold energy [€/MWh], while p^{Cap} is the daily revenue for the capacity reserved during the availability hours [€/MW].

The second-stage cost in Eq. (45) considers the operational expenses expected in each scenario. Imbalance fees ($Cost^{imb}_{t,s}$) are calculated considering the economic flows in case of positive or negative imbalances, represented by c^{+}_{t} and c^{-}_{t}, respectively. The second term of Eq. (45), $Cost^{disc}_{t,s}$, evaluates the payments that the VPP owner owes users in the case of a reduction in their thermal comfort as a consequence of the power management of their water heaters (i.e., when $z^{b,min}_{t,s,n_b}$ or $z^{b,Max}_{t,s,n_b}$ are equal to 1). For each time step in which the water heater temperature is below or above the given thresholds, a fee equal to c^{min} or c^{Max} is paid to the users.

$$minF^{obj,DAM} = Cost^{S1} + \sum_{s \in \mathbb{S}^{DAM}} \pi_s Cost^{S2}_{s} \tag{43}$$

where:

$$\text{Cost}^{S1} = \underbrace{-z^{cap} p^{cap} Cap}_{\text{Rev}^{cap}} + \sum_{t \in \mathbb{T}^{DAM}} \underbrace{c^{buy}_{t} P^{buy}_{t} - p^{sold}_{t} P^{sold}_{t}}_{\text{Cost}^{DAM}_{t}} \tag{44}$$

$$\text{Cost}^{S2}_{s} = \sum_{t \in \mathbb{T}^{DAM}} \underbrace{[c^{+}_{t} \text{Imb}^{+}_{t,s} + c^{-}_{t} \text{Imb}^{-}_{t,s}}_{\text{Cost}^{imb}_{t,s}} + \underbrace{\sum_{n_b \in \mathbb{N}^{B}} (c^{\min} z^{b,\min}_{t,s,n_b} + c^{Max} z^{b,Max}_{t,s,n_b})]}_{\text{Cost}^{disc}_{t,s}} \tag{45}$$

In the next section, the rolling horizon stochastic programming approach developed to manage the operation of the VPP is described.

3.2. Real-time operation

On the delivery day D ($\forall t_{act} \in \mathbb{T}^{D}$), every quarter of an hour, the rolling horizon stochastic programming procedure is executed to dispatch the available power control resources to respect the markets' commitment (DAM + AS requests) and satisfy the users' requests (EV charging and water heating). Flexible resources are scheduled based on their actual status, the forecasts for the future, and corresponding uncertainties. For this purpose, a moving time window is considered. For the optimization performed at t_{act} (actual time step), it is composed of the current time step and a predictive control horizon ($\mathbb{T}^{PC} = [t_{act} + 1; t_{act} + \Delta T_{RH}]$), where ΔT_{RH} is the length of the sliding window [31].

The representation of the procedure is depicted in Fig. 4. At each time step, the architecture receives the current status of VPP resources and, during the availability hours, the AS request from the TSO (blue box in Fig. 4). Starting from these data, several forecasts of the uncertain parameters are generated. In particular, each time series relevant to an uncertain quantity (e.g., $\widetilde{P^{PV}_{t}}$) is composed of the data measured at the actual time ($\widetilde{P^{PV}_{t=t_{act}}}$ which is known without errors) and several forecasts (one for each stochastic scenario) of its evolution in the predictive control horizon (red box in Fig. 4). Then, the predictions of the different parameters (e.g., $\widetilde{P^{PV}_{t,s}}$, $\widetilde{P^{L}_{t,s}}$, $\widetilde{w^{cns}_{t,s,n_b}}$, etc.) are combined to generate scenarios (the detailed description of the procedure is provided in Section 5.2). Therefore, each scenario $s \in \mathbb{S}^{RT}$ collects an expected realization of all uncertainties in the following time steps. Finally, the optimal control of the resources in t_{act} is obtained by solving a two-stage stochastic model. The first-stage collects the decision variables related to the current time (t_{act}), since they must be set before the realization of the uncertain data, while the second-stage considers the predicted operation in the future (orange box in Fig. 4).

The equations that follow are applied to the moving time window, composed of the current time step and the predictive control interval, $\forall t \in t_{act} \cup \mathbb{T}^{PC}$. Once the solution is obtained, the control decisions for the current time t_{act} are applied to the flexible resources and the time window is shifted forward by 15 min.

To model the ESS in the real-time scheduling strategy, Eq. (5)–(10) are applied. Moreover, it is also necessary to include in the formulation some non-anticipativity constraints [32]. They guarantee that, at the current time (t_{act}), decisions are carried out strictly on the basis of information presently available. Eq. (46) and (47) fulfill this task, by ensuring that ESS power exchanges at the present time ($P^{ch,ESS}_{t_{act},s,n_e}$/$P^{ds,ESS}_{t_{act},s,n_e}$) are equal in all the scenarios (i.e., $P^{ch,ESS,FS}_{t_{act},n_e}$/$P^{ds,ESS,FS}_{t_{act},n_e}$, being first-stage

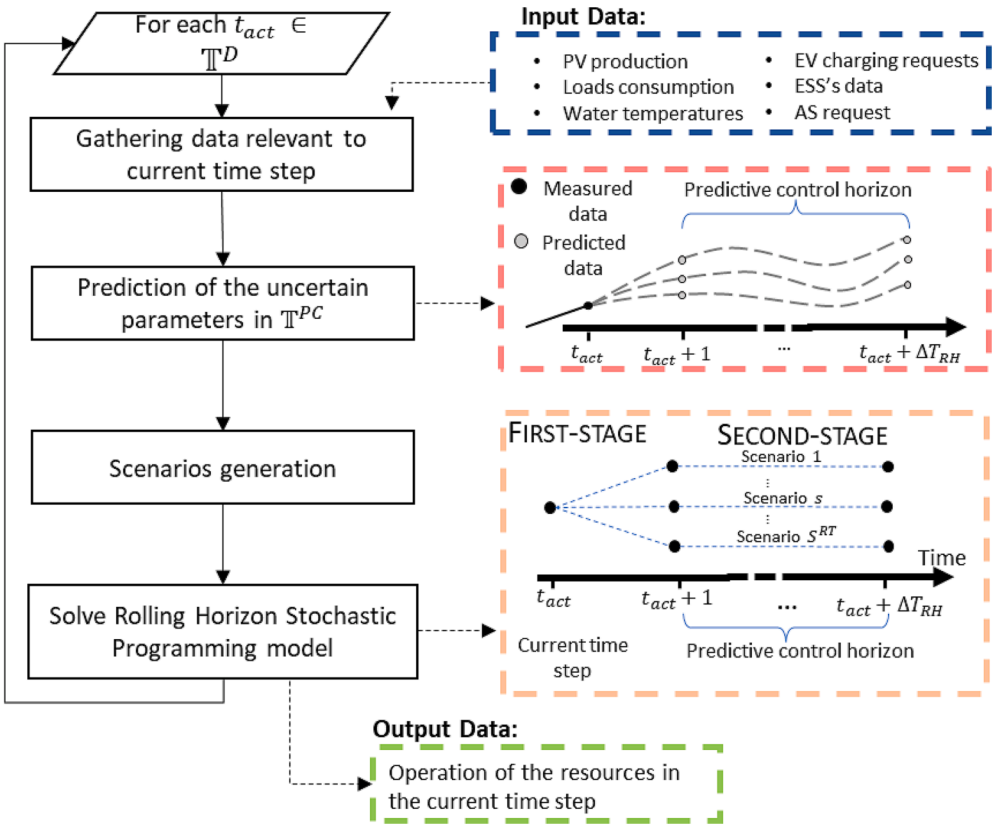

Fig. 4. Structure of the proposed rolling horizon stochastic programming real-time scheduling strategy.

variables, do not depend on the scenarios index). In the following, all the non-anticipativity auxiliary variables will be indicated by introducing the superscript 'FS' (e.g., $P^{ch,ESS,FS}_{t_{act},n_e}$).

$$P^{ch,ESS}_{t_{act},s,n_e} = P^{ch,ESS,FS}_{t_{act},n_e} \qquad \forall s \in \mathbb{S}^{RT} \tag{46}$$

$$P^{ds,ESS}_{t_{act},s,n_e} = P^{ds,ESS,FS}_{t_{act},n_e} \qquad \forall s \in \mathbb{S}^{RT} \tag{47}$$

It can be easily verified that by enforcing Eq. (46) and (47), also the battery SoCs and the total power exchanged at time t_{act} also comply with non-anticipativity constraints.

In addition, the amount of reserve offered through the ESS on the ASM during the availability hours is also checked. For this purpose, Eq. (11)–(14) are adopted to calculate the available ESS's reserve margin ($\Delta P^{ESS,TOT}_{t_{avb},s}$). This ensures that, in case of AS requests, the VPP has an adequate margin available to provide the service activated by the TSO.

At each time step, data relevant to the EVs connected to a CS (initial SoC and vehicle's characteristics) are supposed to be known (e.g., acquired through a communication channel with the CS), while the number of expected EVs charging requests and their data (SoC, charging deadline, etc.) are predicted based on historical data (see Section 5.2). Already connected and predicted EVs are modeled using Eq. (15)–(18). The following non-anticipativity constraint is applied:

$$P^{EV}_{t_{act},s,n_{ev}} = P^{EV,FS}_{t_{act},n_{ev}} \qquad \forall s \in \mathbb{S}^{RT} \tag{48}$$

where, $P^{EV,FS}_{t_{act},n_{ev}}$ represents the charging power of the n_{ev}-th EV at the current time and Eq. (48) forces it to be equal in all scenarios. To evaluate the EV's reserve margin, Eq. (20)–(23) are applied.

The water heater model is based on Eq. (24)–(27), while the users' thermal comfort and the heater flexibility are calculated by Eq. (28)–(30), and Eq. (31)–(34), respectively. The non-anticipativity constraint is given by:

$$P^{b}_{t_{act},s,n_b} = P^{b,FS}_{t_{act},n_b} \qquad \forall s \in \mathbb{S}^{RT} \tag{49}$$

For the real-time scheduling problem, energy imbalances $Imb_{t,s}$ are defined by Eq. (50), as the difference between the markets' commitment (P^{req}_t) and the overall VPP power exchange ($P^{Abs,RT}_{t,s}$). The latter term is calculated considering Eq. (52) and evaluates the power absorbed ($P^{Abs,RT}_{t,s} > 0$) or injected ($P^{Abs,RT}_{t,s} < 0$) into the grid. P^{req}_t is the sum between the DAM schedule (P^{DAM}_t) and the AS requests (P^{AS}_t). P^{DAM}_t is obtained by solving the model described in Section 3.1 and P^{AS}_t is supposed to be communicated to the VPP by the TSO just before the time of delivery. Eq. (37)–(40) are adopted to distinguish positive ($Imb^{+}_{t,s}$) and negative ($Imb^{-}_{t,s}$) imbalances, and Eq. (53) and (54) implement the non-anticipativity constraints.

$$Imb_{t,s} = P^{req}_t - P^{Abs,RT}_{t,s} \tag{50}$$

$$P^{req}_t = P^{DAM}_t + P^{AS}_t \tag{51}$$

$$P^{Abs,RT}_{t,s} = P^{ESS,abs}_{t,s} + P^{EV,abs}_{t,s} + P^{b,abs}_{t,s} - \widetilde{P^{PV}_{t,s}} + \widetilde{P^{L}_{t,s}} \tag{52}$$

$$Imb^{+}_{t_{act},s} = Imb^{FS,+}_{t_{act}} \qquad \forall s \in \mathbb{S}^{RT} \tag{53}$$

$$Imb^{-}_{t_{act},s} = Imb^{FS,-}_{t_{act}} \qquad \forall s \in \mathbb{S}^{RT} \tag{54}$$

To drive the real-time optimization process (i.e., to adjust the power exchange of the flexible resources in the VPP instant by instant), the following objective function is applied:

$$\min F^{obj,RT} = \mathrm{Cost}^{RT,S1} + \sum_{s \in \mathbb{S}^{RT}} \pi^{RT}_s \mathrm{Cost}^{RT,S2}_s \tag{55}$$

where the first term ($Cost^{RT,S1}$) represents the actual costs experienced by the VPP at the current time (Eq. (56)), while $Cost^{RT,S2}_s$ evaluates

the cash flows expected in the future (Eq. (57)). Finally, during the availability hours t_{avb}, the EMS verifies the availability of the reserved capacity (Cap) by Eq. (41) and (42).

The VPP is paid for the reserve margin made available to the TSO during the availability hours; the term Rev_s^{Cap} is introduced in Eq. (57) to check its actual provision.

$$\mathrm{Cost}^{RT,S1} = \underbrace{c^{+}_{t_{act}} Imb^{+}_{t_{act}} + c^{-}_{t_{act}} Imb^{-}_{t_{act}}}_{\mathrm{Cost}^{imb}_{t_{act},s}} + \underbrace{\sum_{n_b \in \mathbb{N}^B} \left(c^{\min}\, z^{b,\min}_{t_{act},n_b} + c^{Max} z^{b,Max}_{t_{act},n_b}\right)}_{\mathrm{Cost}^{disc}_{t_{act},s}} \tag{56}$$

$$\mathrm{Cost}^{RT,S2}_{s} = \sum_{t_s \in T^{PC}} \left[\underbrace{c^{+}_{t_s} Imb^{+}_{t_s,s} + c^{-}_{t_s} Imb^{-}_{t,s}}_{\mathrm{Cost}^{imb}_{t_s,s}} + \underbrace{\sum_{n_b \in \mathbb{N}^B} \left(c^{\min}\, z^{b,\min}_{t_s,s,n_b} + c^{Max} z^{b,Max}_{t_s,s,n_b}\right)}_{\mathrm{Cost}^{disc}_{t_s,s}} \right] - \underbrace{p^{Cap} Cap\left(z^{cap}_{s}\right)}_{Rev^{Cap}_{s}} \tag{57}$$

The model was designed to be solved in a real-time configuration, so its runtime is key. To reduce the computational requirement of each run, the optimal second-stage variables were saved and used as first-guess solution in the next time step.

4. Case study

To test the performance of the proposed strategy, a realistic case study was defined. For this purpose, a VPP composed of 100 residential customers was considered, each one equipped with a rooftop PV power plant (3.3 kW of peak power) and a water heater. The PV nominal power was chosen according to the most widespread size for residential applications [33]. The PV production and the relevant day-ahead forecast were based on real data collected from a power plant located in Central–Northern Italy, obtaining an annual production of approximately 4,600 kWh/user. The yearly average day-ahead forecast error of PV production was approximately 6.5%. The non-flexible load profiles were derived from data gathered on 100 real residential customers [34], while the day-ahead forecast value was evaluated by adopting a persistence model (the day-ahead forecast error was equal to 7.2%). The annual energy consumption of non-flexible loads was approximately 2,400 kWh/user, while the average user consumption also considering EVs and water heaters was 4,300 kWh/user. In Fig. 5, PV and non-flexible load profiles are shown for 4 representative days, one for each season.

Each water heater was characterized by a volume (V_{n_b}) of 100 L and a nominal power ($P^{n,nom}_{n_b}$) of 1.5 kW. The hot water usage was modeled based on the approach proposed in [35], while the fees in case of comfort reduction c^{min} and c^{Max} were set equal to 1 € and 0.5 €, respectively, for every quarter of an hour in which the temperature was outside the allowed range [36]. It was assumed that half of the houses were equipped with a stationary ESS ($C^{ESS}_{n_e} = 5$ kWh, $P^{ESS}_{n_e} = 3$ kW, and $\eta^{ch} = \eta^{ds} = 0.92$) and an EV charging station ($P^{CS}_{n_{ev}} = 6$ kW). The EV's usage and the corresponding charging request were simulated by adopting the model described in [37], while the battery capacity of each EV ($C^{EV}_{n_{ev}}$) was defined considering the technical characteristics of the best-selling models in Italy [38].

The AS requests were reproduced through the historical data collected on the Italian ASM [39]. To this purpose, all the upward reserve bids submitted in the ASM were considered in terms of price and power rewarded. Then, it was assumed that the TSO activated the VPP's reserve according to a merit order approach: the capacity was activated if the price offered by the VPP (fixed to 200 €/MWh during the entire year) was lower than the highest price accepted by the TSO. In the case of AS provision, a pay-as-bid approach was adopted (the VPP was paid 200 €/MWh). The remuneration for the upward reserve offered was set to $p^{Cap}_t = 18$ €/MW for each hour of availability (i.e., approximately 20,000 €/MW/year, in line with the actual prices registered for this service in Italy). The amount of regulating reserve made available by the VPP (Cap) is assumed equal to 50 kW, calculated with the procedure proposed in [36], considering the trade-off between economic benefits and reliability of the reserve availability. In Italy, the regulation reserve (Cap) is supposed to be required in the period 3 pm–6 pm (i.e., availability hours) [23].

The cost/price for the energy purchased/sold (c^{buy}_t and p^{sold}_t) were calculated by averaging the actual DAM data of 2022, as 300 and 200 €/MWh, respectively. The uncertainty of DAM prices was not assessed in this work, hence c^{buy}_t and p^{sold}_t were considered constant and fully deterministic.

The imbalances are subject to a single price mechanism [30], hence, if a mismatch between the power exchanged and the power scheduled (DAM + AS) is detected (i.e., $Imb \neq 0$), the difference is penalized at c^{+}/c^{-}, which is set equal to $-0.5 \cdot p^{sold}_t = -100$ €/MWh and $+0.5 \cdot p^{sold}_t = 100$ €/MWh, respectively [40].

Finally, the time resolution adopted for numerical simulations was equal to 15 min, while the length of the predictive control horizon (ΔT_{RH}) was set to 1 h (i.e., four time steps).

5. Scenario generation

The models required suitable scenarios to represent the realization of

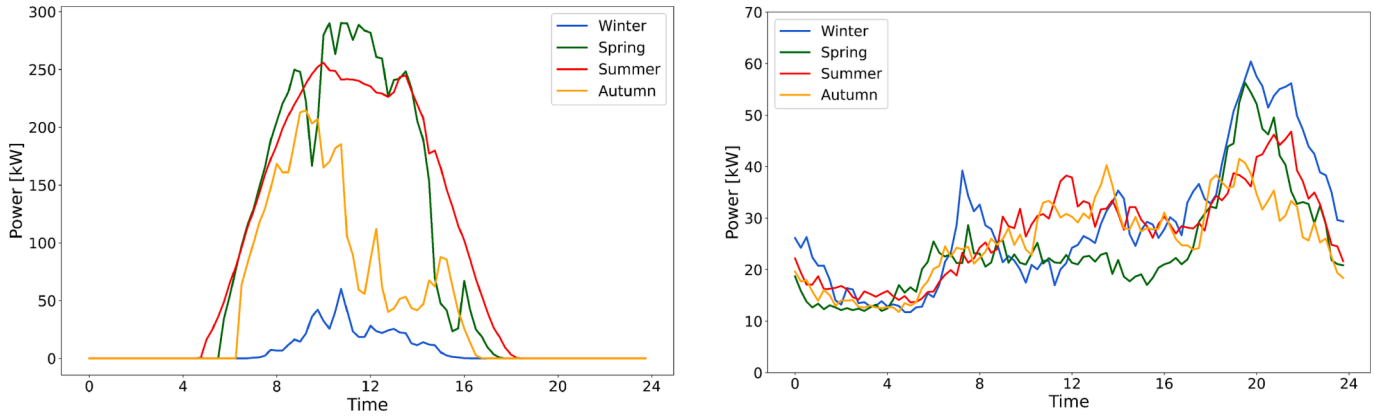

Fig. 5. PV production (left) and non-flexible loads absorption (right) in four representative days.

the second-stage uncertainties. This section describes the procedures to generate the scenarios for the DAM participation and real-time operation.

5.1. DAM uncertainty characterization

During the DAM bidding process, the uncertainties affecting PV production and non-programmable loads ($\widetilde{P^{PV}_{t,s}}$ and $\widetilde{P^{L}_{t,s}}$ in Eq. (36)), hot water usage ($\widetilde{w^{cns}_{t,s,n_b}}$), and EV charging requests ($\widetilde{h^{EV,con}_{t,s,n_{ev}}}$ and $\widetilde{\Delta SoC^{usg}_{t,s,n_{ev}}}$) were considered. To originate the scenarios for the stochastic model, the following steps were carried out, as exemplified in Fig. 6:

1. For each uncertain parameter, here denoted by X, where X could be $\widetilde{P^{L}_{t}}$, $\widetilde{P^{PV}_{t}}$, $\widetilde{w^{cns}_{t,n_b}}$, $\widetilde{h^{EV,con}_{t,n_{ev}}}$ and $\widetilde{\Delta SoC^{usg}_{t,n_{ev}}}$, the expected profile for the next day (X^{F}_{t}) was forecasted. Which method was adopted to elaborate the prediction was irrelevant for the application of the procedure, and its development was outside of the scope of this study.
2. An iterative procedure was performed. At each iteration i, an error $\epsilon^{X}_{t,i}$ was added to the forecasted profile (see Eq. (58)). $\epsilon^{X}_{t,i}$ was generated by adopting an ARMA model [41], trained considering the forecast errors detected during the previous days. In this research, 5 ARMA models were used, one for each parameter (i.e., $X \in \{\widetilde{P^{L}_{t}}, \widetilde{P^{PV}_{t}}, \widetilde{w^{cns}_{t,n_b}}, \widetilde{h^{EV,con}_{t,n_{ev}}}, \widetilde{\Delta SoC^{EV,usg}_{t,n_{ev}}}\}$), and the optimal order of each ARMA model was obtained by adopting Akaike's information criterion [42].

$$\widetilde{X_{t,i}} = X^{F}_{t} + \epsilon^{X}_{t,i} \tag{58}$$

3. The uncertain parameters relevant to non-energetic quantities (i.e., hot water usage and EV charging requests) were transformed into equivalent power profiles by considering their average power absorption, estimated by data collected on previous days. Several scenarios of realization were defined by randomly selecting a power profile for each uncertain parameter. The overall expected power profile was calculated for each scenario as the sum of the different resource contributions (i.e., PV system + load + water heater + EV).
4. A k-means scenario reduction was applied to the power profiles previously obtained, selecting K representative trends among all of the available ones. To evaluate the number of clusters to adopt (K), the silhouette method was applied [43,44].
5. A random power profile was selected as representative among the population within each cluster. Finally, the initial uncertain parameters (i.e., $\widetilde{h^{EV,con}_{t,s,n_{ev}}}$, $\widetilde{\Delta SoC^{EV,usg}_{t,s,n_{ev}}}$ and $\widetilde{w^{cns}_{t,s,n_b}}$) having generated the representative profile were used in the second-stage problem of the model described in Section 3.1.

5.2. Real-time uncertainty characterization

The real-time management of the VPP was based on a two-stage stochastic model; therefore, the uncertainties affecting short-term decisions also needed to be characterized with a scenario-based approach. The development of short-term forecast algorithms is outside of the scope of this study; thus, straightforward methodologies were adopted to estimate the evolution in the predictive control horizon. It is important to underline that the EMS optimization approach proposed in Section 3 does not rely on a specific forecasting method and different methods could be more suitable in other situations.

Short-term forecasts for load and PV were conducted using ARMA models, similar to those described in [45] and [46]. The ARMA models were applied to the values measured in previous time steps to obtain forecast profiles for each scenario. It should be noted that ARMA models require time series to be stationary [47], which is rarely satisfied by PV production and load consumption data. For this reason, the approach adopted in [48–50] was utilized. The data were subdivided into smaller groups to satisfy the stationary requirement. In particular, the training datasets, composed of the quarter-hour measurement of the PV system and loads, were firstly grouped by season to mitigate the seasonality effects. Then, within each seasonal group, the daily production profiles were further subdivided into 6 subgroups, each one containing the PV production data for four consecutive hours of the day. Therefore, a total of 24 subgroups were defined for both PV production and load consumption data (24 + 24 = 48 profiles in total).

The Kwiatkowski-Phillips-Schmidt-Shin and Augmented Dickey-Fuller tests were performed in parallel to assess the stationarity behavior of each subgroup [51]. The results of both tests confirmed the hypothesis of stationary time series, thereby validating the adoption of ARMA models. It is worth noticing that, if the time series were not stationary, the adoption of more complex approaches such as ARIMA or machine learning models should be required. Finally, for each subgroup, an ARMA model was trained. Therefore, in total, 48 ARMA models were defined. For each one, the coefficients were optimized using the "pmdarima" package [52].

Fig. 7 shows the improvement of the forecast accuracy provided by the proposed ARMA models compared with the day-ahead forecast. In particular, the black line depicts the load and PV forecast relative error (i.e., ratio between the error in kW and the measured value) made during the DAM participation (i.e., 24 h in advance). The colored lines refer to the forecast refinement performed, getting closer to the real time

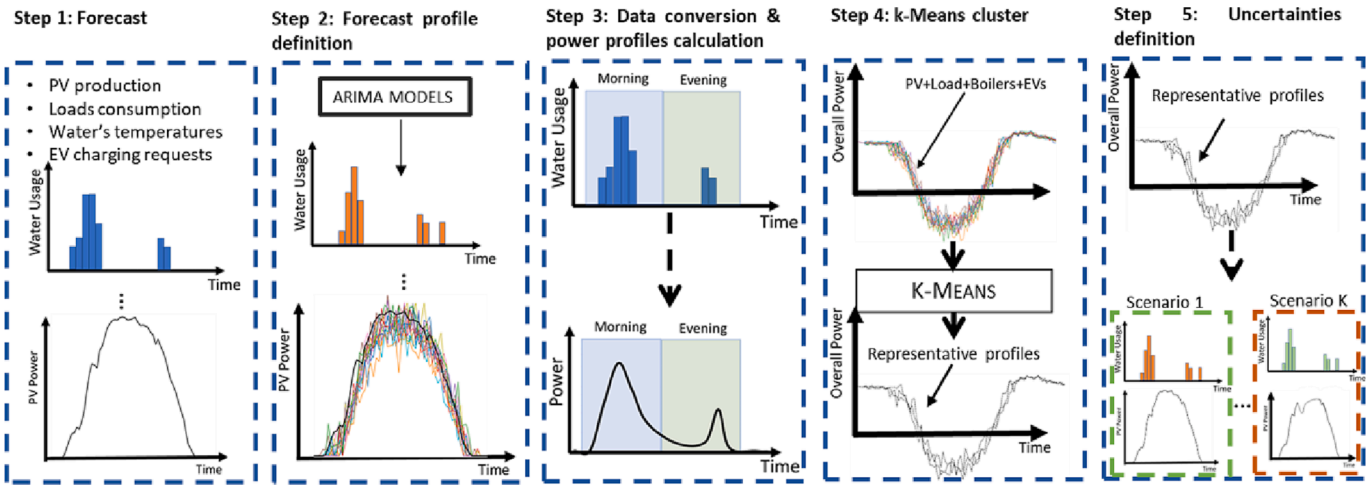

Fig. 6. Scenario generation procedure.

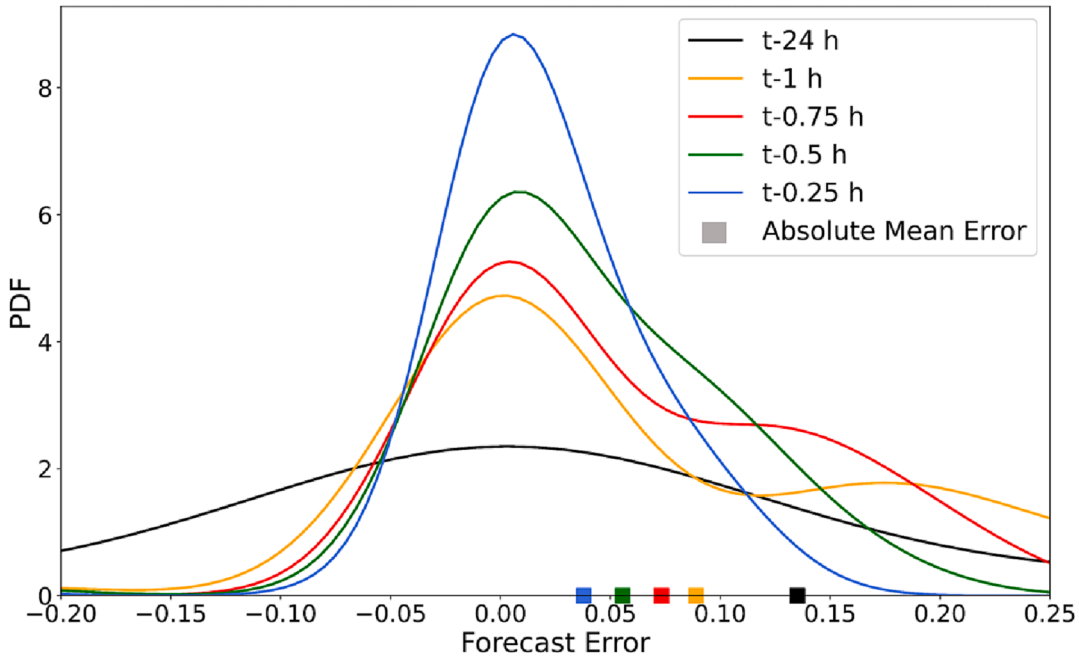

Fig. 7. PDFs of the load and PV relative forecast error. The square markers represent the absolute mean forecast error.

(15, 30, 45, and 60 min before the current time). Colored squares represent the average values of the absolute error detected over the period considered. As can be seen, the mean absolute day-ahead forecast error (13.8%) was approximately 3.9 and 1.9 times higher compared with the forecast performed 15 and 45 min in advance (3.5% and 7.2%), respectively. Furthermore, the forecast refinement performed closer to real time allowed a lower presence of larger forecast errors, as is shown by the reduction in the PDFs tails.

Instead, the water consumption forecasts were based on a random walk persistence model; the value expected in the following time steps was set as being equal to the last value measured plus a normally distributed error. The approach used was justified by the fact that, according to the analyses carried out, the water usage samples only showed a good correlation with the value of the previous (15 min in advance) time step [41].

Vehicle charging requests were estimated based on the historical data collected during the previous days. The approach drew the expected number of charging requests in the upcoming time steps and the SoC on arrival from the corresponding PDFs. A detailed description of the approach is reported in [53].

Finally, by randomly combining a forecast for each parameter, the scenarios of the rolling horizon stochastic programming problem described in Section 3.2 are defined.

6. Model implementation: An illustrative example

In this section, a detailed description of the VPP operation for one day in spring was presented to clarify the operating logic and benefits of the EMS. Then, in Section 7, an extensive analysis of the EMS performance and a sensitivity analysis regarding the number of scenarios was performed.

The day analyzed was characterized by variable weather conditions (i.e., large forecast errors), making the EMS operation more challenging. This case considered 11 stochastic scenarios (i.e., the cardinality of $\mathbb{S}^{RT}$ was 11).

DAM scenarios were created with the approach described in Section 5.1. A day-ahead forecast for each uncertain parameter was considered and, through the iterative procedure described in step 2 of Section 5.1, 300 scenarios were generated and clustered by the k-means algorithm. The number of clusters selected by the silhouette method was 15 (i.e., cardinality of $\mathbb{S}^{DAM} = 15$).

In each scenario selected by the k-means method, the optimal DAM profile and upward reserve were defined by solving the model described in Section 3. Fig. 8 shows the DAM binding schedule and the upward reserve offered on the ASM (orange bars). It was observed that, during the availability hours (3 pm–6 pm; green area), the VPP offered a quota of upward reserve that was always higher than *Cap* (red horizontal line). Hence, the VPP received the reserve availability remuneration.

For each time step of the delivery day, the second layer of the EMS (i.e., rolling horizon stochastic programming model) was executed. As is described in Section 3.2, the EMS forecasted the evolution of the uncertain parameters in the predictive control horizon based on the current measurements. Fig. 9 shows the comparison between the actual PV production (in red) and the one forecasted 15 min before the time of delivery; the latter was used by the EMS to perform real-time scheduling and is represented as range (in blue) between the maximum and minimum value forecasted on all 11 scenarios. Despite the simple forecast model adopted and the variable weather conditions, the proposed method predicted the PV production trend quite accurately, refining the forecast used during the DAM bidding (black dotted line in Fig. 9). It is worth noting that the day-ahead PV forecast was not particularly accurate, making it more complex for the second layer of the EMS to follow the DAM commitment.

According to the short-term forecasts and the corresponding scenarios, the optimal dispatch of available regulating resources was obtained. Fig. 10 shows the resulting energy flows (colored bars) and the ESS's SoC trend (dotted line) on the day analyzed. As can be seen, most of ESSs and water heater absorptions (violet and green bars, respectively) occurred in the early morning and during the PV system peak hours (approximately 2 pm). This can be interpreted by considering that these two systems were used by the EMS logic with a twofold scope: *i*) to maximize the energy self-consumed by the VPP by performing a time shift of the energy required and produced, and *ii*) to reduce the forecast errors and provide ASs (between 6 and 8 am the PV production is higher than the value forecasted during the DAM bidding, see Fig. 9; thus, ESSs and water heaters were used to compensate for this error). Similarly, the EV power absorptions (magenta bars) mainly occurred in the afternoon hours (2:30–4:30 pm) to exploit PV production, thus maximizing the

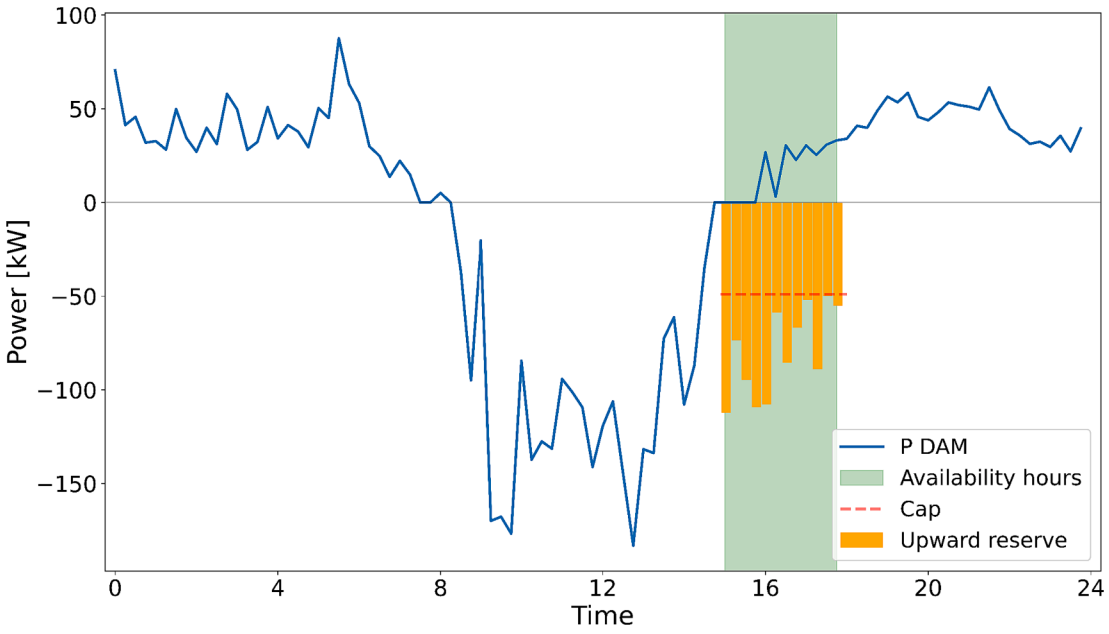

Fig. 8. DAM power schedule for the day under analysis and the upward reserve availability.

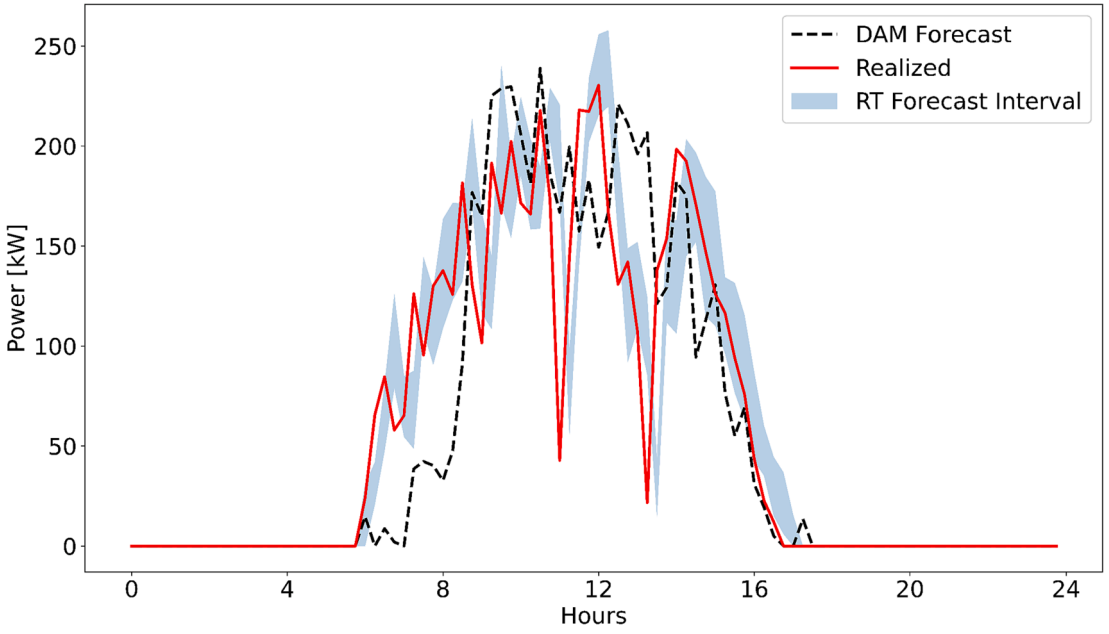

Fig. 9. Comparison between the measured PV production (red line), the day-ahead forecast (dotted line), and the forecast range adopted for the real-time scheduling (blue area).

self-consumed energy. Then, the EV charging was completed during the late evening (6:00–10:30 pm), exploiting the energy stored in the batteries (see the SoC profile in Fig. 10). This ensured an adequate charging profile before the vehicles' departure.

In Fig. 10, the PDFs of the EVs' SoC at the charging station arrival and departure time are shown in blue and orange, respectively. Despite the large variability in the initial SoC, which ranged between 0.45 and 0.83, and the connection deadline uncertainties, the EMS suitably charged the EVs prior to their departure. In fact, the mean SoC on departure was 0.96 (and was therefore very close to being fully charged), while the EVs that left the charging stations with an SoC of$<$0.80 only represented 1.0% of the total. Finally, in the last plot of Fig. 10, the PDF of the temperature of the water heaters is shown. In 93% of cases, the temperature was inside the range of comfort (shown by the two vertical lines). In the remaining cases (7%), even if the temperature was outside of the optimal range, the average temperature (54.6 °C) was only approximately 5 °C lower than the 60 °C threshold; in addition, the probability of reaching a temperature lower than 40 °C (considered the minimum acceptable temperature for the user [54]) is only 0.2%.

The overall power exchange of flexible resources was managed to minimize the power mismatch (shown in Fig. 10 by red markers) with respect to market commitments (DAM + AS provision). Despite the variable weather conditions and corresponding day-ahead forecast errors, the total energy imbalance during the day was only 62.7 kWh, which is$<$3.5% of the total energy absorbed by the VPP (1,775 kWh). Moreover, the imbalance's peak power (50 kW at 12 pm) was three

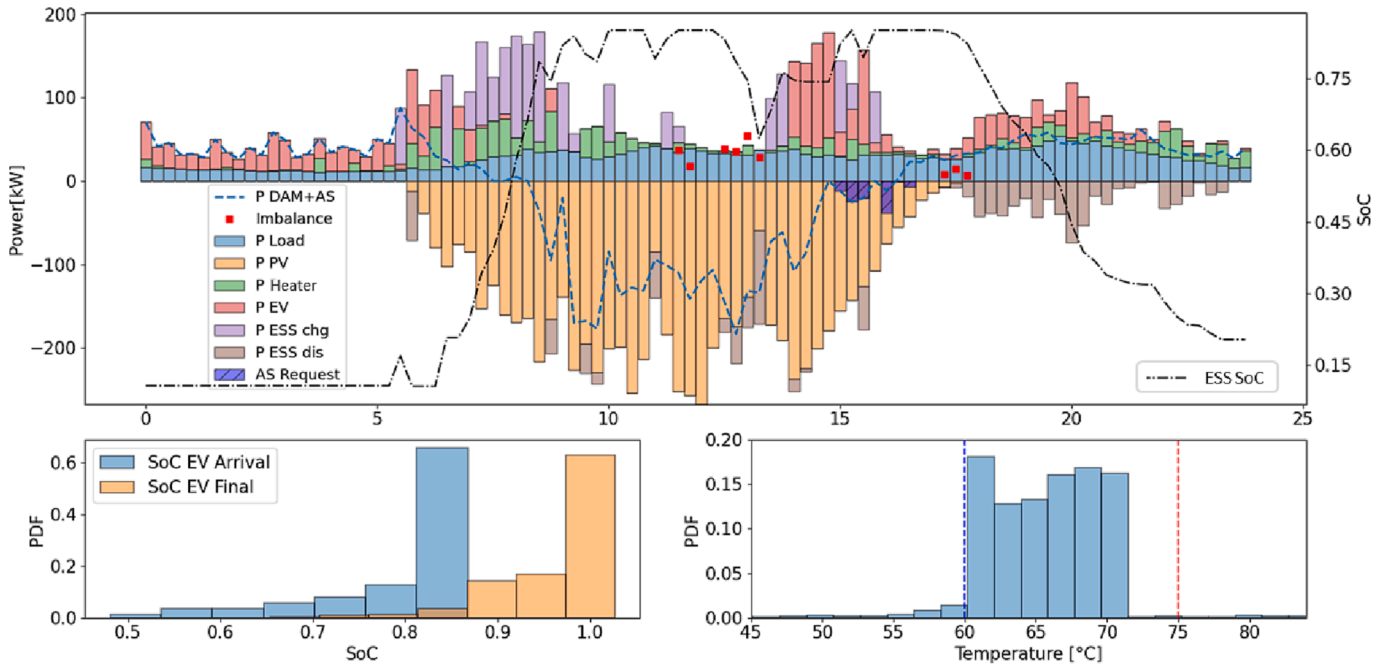

Fig. 10. Power flows in the VPP (above) and PDFs of the EVs' SoC and water temperatures (below) over the day of simulation.

times lower than the maximum day-ahead PV forecast error (i.e., the difference between the power forecasted and the power produced), which was 152 kW at 11:00 am (see the distance between the red and black lines in Fig. 9).

Finally, some considerations can be drawn on the capability of the EMS to reserve the regulation band required and provide ASs. Just before the availability hours (approximately 2 pm), the EMS charged the ESSs to ensure the reserve margin offered on the ASM. This is because the rolling-horizon-based approach predicted the evolution of the VPP in the following hours and, thanks to Eq. (41) and (42), ensures to make available the capacity needed on the ASM was made available.

As is shown by the hatched violet bars, the TSO requested that the VPP reserved flexibility for 1.25 h on the selected day, requiring a maximum power variation of 40 kW (maximum regulation reserve *Cap* = 50 kW). During the service provision, no power imbalances were detected; hence, the reserve activation was perfectly satisfied by the TSO.

7. Validation of the rolling horizon stochastic programming model

This section proves the effectiveness of the proposed EMS and quantifies the effect of the short-term uncertainties during the VPP's operation. Three different case studies were analyzed, which differed in the approach adopted to manage the resources in real time (i.e., second layer of the EMS), but kept the DAM and ASM bidding process unchanged (the model in Section 3.1). These were:

- *RH Stc n* case*:* The proposed rolling horizon stochastic programming model was implemented. A sensitivity analysis of the number of scenarios (n) considered during the real-time dispatch (i.e., cardinality of $\mathbb{S}^{RT}$) was also provided.
- *RH Det* case: Here, the real-time dispatch was obtained without considering the effects of uncertainties; therefore, the VPP operation was obtained considering only the average scenario (i.e., cardinality of $\mathbb{S}^{RT} = 1$). In the literature, this case study has usually been referred to as rolling horizon optimization and it is considered a state-of-the-art approach to schedule an asset of energy resources [55].
- *RH Omn* case*:* This assumes that the second layer of the EMS can perfectly forecast the uncertain parameters inside the predictive control horizon (i.e., omniscient prediction 1 h in advance). This case study was designed to provide an ideal upper bound on the performances of the EMS second layer. It is worth noting that the uncertainties during the DAM participation were still present because the goal of this analysis was to assess the impact of unexpected events only during the real-time dispatch.

Table 2 reports the VPP results obtained in four representative weeks (one per season). To ensure a fair comparison, the same input data, including PV production, loads absorption, water usage, EV charging requests, and AS activations, were used in all of the case studies. Thus, the net energy exchanged in the DAM and corresponding revenues were almost constant in all scenarios (see the 4th row in Table 2). The small differences (lower than 1.5%) can be attributed to the different exploitation of the storage units in real time and the corresponding internal energy losses.

Concerning the capabilities of the three models to respect the markets' commitment, the first column of Table 2 shows the average daily energy imbalance detected. The highest value was observed in the *RH Det* case study (198.7 kWh/day), while the proposed rolling horizon stochastic programming model allowed this to be drastically reduced, reaching 148.69 kWh/day in the case study with 13 scenarios. Therefore, considering the short-term uncertainties during the real-time dispatch allowed the imbalances to be reduced by up to 25.17% compared with a deterministic model (i.e., *RH Det*). Even in the ideal case (*RH Omn*), an average imbalance of 81.58 kWh/day was detected. This is because the day-ahead forecast uncertainties were still present.

The EMS relies on the EVs' charging flexibility and the thermal inertia of water heaters to mitigate imbalances and make available reserve margin to the grid. Therefore, the effects on the services offered to users must be also evaluated. Concerning e-mobility, it can be seen that, by increasing the number of scenarios, the average SoC at the vehicle departure remained almost constant. However, the percentage of EVs that left the CSs with a low SoC decreased considerably; in the deterministic case study (*RH Det*), 20% of EVs were released with a SoC < 0.90 and the 10th percentile of the final SoC was 0.86 (i.e., 10% of EVs were released with a SoC < 0.86). When adopting the proposed

Table 2
Techno-economic results in the analyzed case studies.

Case Study	Technical Results			Economic Results				
	Energy Imbalance [kWh/day]	Water Temperature [°C]	EVs' Final SoC	DAM Revenues [€/day]	Imbalance Cost [€/day]	ASM Revenues [€/day]	Discomfort Cost [€/day]	Total Operation Cost [€/day]
RH Omn	81.58	62.4 [60.1; 63.5]	0.98 [0.97; 1]	−134.69	8.16	−3.59	0	4.57
RH Det	198.71	61.6 [58.7; 65.6]	0.97 [0.86; 1]	−138.65	19.87	−3.59	14.38	31.16
RH Stc 3	205.59	62.8 [59.1; 65.9]	0.97 [0.89; 1]	−139.22	20.56	−3.59	15.14	32.61
RH Stc 5	168.54	64.8 [60.89; 67.8]	0.98 [0.89; 1]	−137.41	16.85	−3.59	9.82	23.09
RH Stc 7	175.44	64.7 [61.1; 67.6]	0.98 [0.92; 1]	−135.05	17.54	−3.59	4.58	18.54
RH Stc 9	152.19	64.6 [61.2; 67.8;]	0.98 [0.93; 1]	−137.59	15.22	−3.59	6.33	17.96
RH Stc 11	149.84	64.5 [61.1; 67.4]	0.98 [0.95; 1]	−136.14	14.98	−3.59	5.35	16.74
RH Stc 13	148.69	64.9 [61.2; 67.8]	0.98 [0.95; 1]	−135.47	14.87	−3.59	5.84	17.11

stochastic approach with 11 scenarios, less than 8% of EVs left the CS with a SoC < 0.90 and the 10th percentile grew to 0.95 (i.e., only 10% of EVs were released with a SoC < 0.95). This result is particularly noteworthy also compared with the *RH Omn* case, in which the charging deadlines were known in advance. In the ideal case, 8% of the EVs were released with a SoC < 0.95 and the 10th percentile was only 2% higher (0.97) compared with the proposed stochastic model. Thus, despite the straightforward approach adopted to forecast the EV charging requests, the outcomes achieved in the *RH Stc* case study were close to ideal (*RH Omn*).

Table 2 shows the statistical properties (mean, 10th and 90th percentiles) of the water temperature in the different case studies. In the stochastic case study (*RH Stc*), the average temperature and 10th percentile were almost 3 °C higher compared with the value obtained in *RH Det*. This is because the stochastic scheduler explored different scenarios of water consumption and opted to preheat the water to avoid an insufficient temperature. On the other hand, the deterministic formulation (*RH Det*) tended to underestimate the water consumption variability in the upcoming time steps, because a single (average) scenario was considered. As a consequence, in the *RH Det* case, each user experienced 15 min of cold water (<55 °C) during every week analyzed, while in the stochastic model (e.g., *RH Stc 11*), the discomfort duration was reduced by 62.8%. In the *RH Omn* case, the water temperature was always inside the comfort range, since the EMS perfectly forecasted water usage in the subsequent time steps. These considerations affected the discomfort costs, which (e.g., *RH Stc 13*) were reduced by almost three times in the stochastic formulation compared with the deterministic approach (*RH Det*).

The ASs requested by the TSO during the simulated period are depicted in Fig. 11 (orange bars). On average, the VPP reserve was activated almost twice per week (7 activations in 28 days). During the AS provision, the mean power activated was 22 kW and, on average, the service provision lasted for 1 h (out of 3 h of availability). However, in some cases (especially during winter and spring days), the AS request

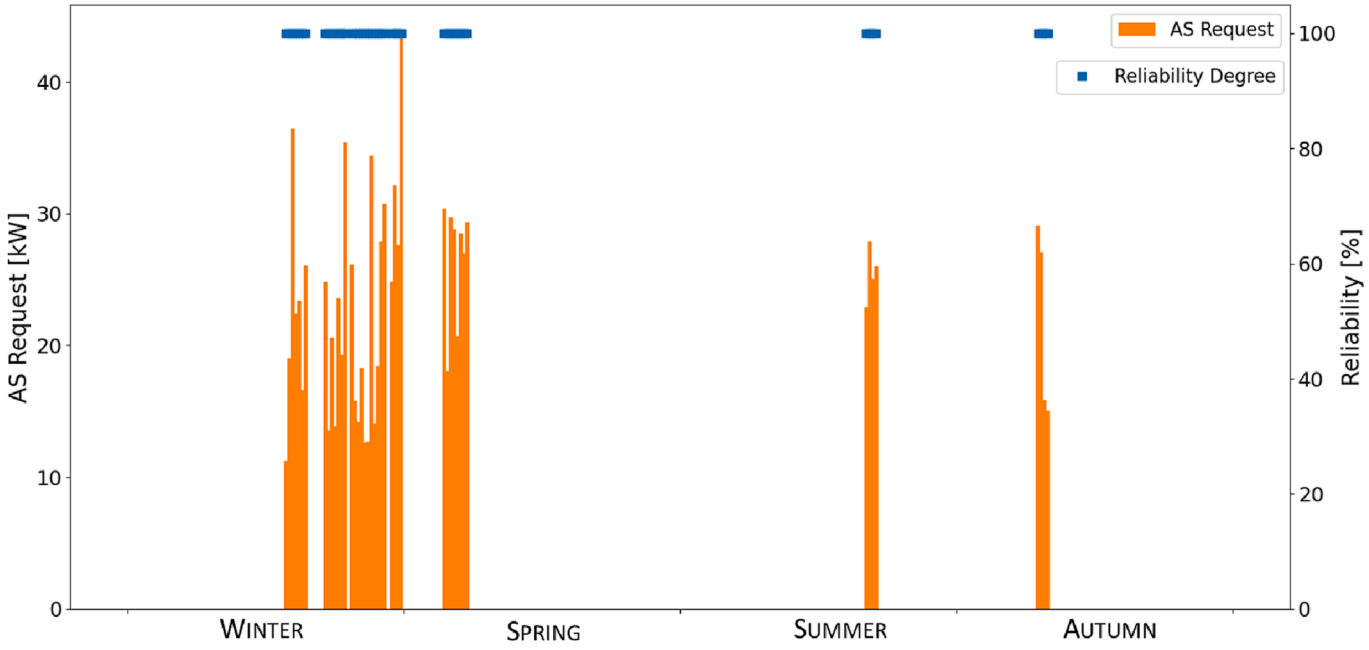

Fig. 11. Upward AS requests activated by the TSO in the 4 weeks simulated (orange bars) and the corresponding degree of reliability (in blue). Only the availability hours are depicted.

lasted up to 3 consecutive hours. Fig. 11 shows the reliability during the service provision, calculated as the ratio between the power variation provided by the VPP and that requested by the TSO. It is worth noting that the reliability of the provision was always 100%; hence, the VPP always provided the requested regulation without imbalances. Furthermore, in all the case studies analyzed, the VPP was always capable of making the upward reserve available (*Cap*).

Finally, an analysis of the economic outcomes of the case studies was provided. Since all the scenarios adopted the same DAM strategy (variation in daily DAM revenues was sufficiently low to be neglected), the analysis focused on the costs arising from the operation of the VPP on day D (see Eq. (56)).

To evaluate the impacts of short-term uncertainty, the value of uncertainties VoU(*n*) was introduced as a metric. This measures the improvement, in terms of operational cost, of adopting a stochastic model rather than a simpler deterministic one; VoU(*n*) is defined as the average variation in the operational cost between the *RH Stc* and *RH Det* case studies, normalized with respect to the average *RH Det* operational cost. Therefore, this index assessed if a deterministic scheduler (*RH Det,* in which the short-term uncertainties were neglected) led to misguided dispatch decisions in a stochastic environment.

Fig. 12 presents the average operational costs (see Eq. (56)) and corresponding 10^{th} and 90^{th} percentiles in the different case studies. According to Fig. 12, the proposed rolling horizon stochastic programming model provided a considerable improvement compared to its deterministic counterpart (*RH Det*). In particular, the adoption of just five scenarios allowed for the average cost to be lowered by approximately 8.07 €/day (23.09 compared with 31.16 €/day); therefore, VoU(5)= − 25.91%. Similarly, solving 11 scenarios introduced a cost saving of 14.42 €/day (16.74 compared with 31.16 €/day), so VoU(11)= − 46.27%. The cost reduction was mainly due to the capability of the stochastic scheduler to drastically reduce the imbalance (− 4.89 €/day w.r.t *RH Det*) and discomfort costs (− 9.04 €/day w.r.t *RH Det*). Instead, revenues arising from offering the reserve and AS provision remained constant in all cases. A similar reduction in costs could also be found by analyzing the *RH Stc 13* case study, where VoU(13)= − 45.07%. However, this scenario was computationally heavy to manage and presents convergence issues during the resolution of the optimization problem. Since the EMS was designed to run almost in a real-time configuration, two stop criteria were adopted during the rolling horizon stochastic programming model resolution (second layer of the EMS). The first was based on the MIP gap (fixed to 0.5%), and the second had a fixed upper limit for the computational time (<120 s for each time step). The *RH Stc 13* case study hit the time limit in almost 13% of runs. Hence, in approximately one-sixth of executions, a sub-optimal solution was used to schedule the regulating resources. Consequently, the average operational costs were not further reduced compared with the *RH Stc 11* case.

The gap of the stochastic scheduler compared with the ideal case (i.e., *RH Omn*) could be quantified by the value of perfect forecast VoPF(*n*) index, defined as the cost variation between the *RH Stc* and *RH Omn* approaches, divided by the *RH Stc* operational cost. The operational cost in the ideal case (*RH Omn*) was − 12.17 €/day lower compared with the *RH Stc 11* case, so VoPF(11) = 75.7%.

The economic profitability of the proposed rolling horizon stochastic programming model was highlighted by the total daily profit, calculated as the sum between DAM revenues (on average equal to − 136.78 €/day) and operational costs. The stochastic approach with 11 scenarios allowed the VPP's revenue to be increased by 11.08% compared with the deterministic scheduler (− 119.39 €/day compared with − 107.48 €/day). Furthermore, the daily revenue in the *RH Omn* case was approximately − 129.35 €/day, which was 20.55% and 8.53% higher than the *RH Det* and *RH Stc 11* cases, respectively.

Finally, the computational times required by the different mathematical models under analysis were compared. Tests were run on a workstation equipped with an Intel Core i9-10980XE processor, 128 GB of RAM, and a Windows 10 operating system. The models were built using Pyomo [56] and solved through the commercial software Gurobi 9.5. In all case studies, the optimization of the DAM schedule (first layer) took approximately 45 s, while the time required to carry out the real-time dispatch (second layer) was influenced by the number of scenarios analyzed. In both the *RH Omn* and *RH Det* case studies, the time required to solve one time step was approximately 4 s (i.e., 6.4 min to simulate the entire day, since a 15 min resolution was adopted). On the other hand, the resolution of the proposed rolling horizon stochastic programming model required, on average, from 12 s (*RH Stc 3*) up to 68 s (*RH Stc 13*) for each time step.

8. Conclusions

In this study, an EMS that optimizes the market bidding and real-time operation of a VPP composed of residential users equipped with small-scale renewable assets, non-flexible loads, and thermal and electrochemical storage systems was developed. The DAM and ASM participations were optimized through a two-stage stochastic model that considered day-ahead uncertainties. The real-time management was

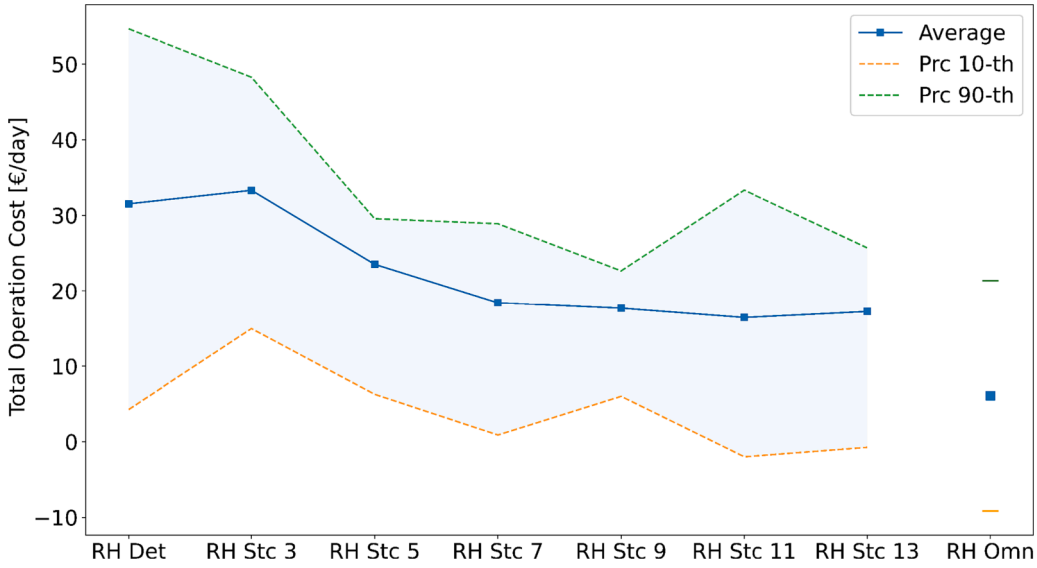

Fig. 12. Trend in the average operational cost (blue line) and corresponding percentiles in the different case studies.

based on an innovative rolling horizon stochastic programming model, optimally dispatching the regulating resources considering the effects of short-term uncertainties.

The extensive simulations performed proved the effectiveness of the approach and allowed for evaluation of the impact of short-term uncertainties on the VPP dispatching. It emerged that the EMS was effective in limiting power imbalances, also providing a reliable balancing reserve margin on the ASM. Moreover, a satisfactory service was guaranteed to be provided to residential users (both in terms of hot water temperature and EV charging).

The comparison of the rolling horizon stochastic programming model with its deterministic counterpart showed that the adoption of a stochastic formulation can bring significant techno-economic benefits compared with the methods that have usually been adopted in the literature. In particular, taking into account the short-term uncertainties, this allowed for a reduction in operational costs of up to 45% and the VPP's total profits increased by 11% compared with the deterministic approach. Furthermore, despite the presence of non-programmable generation (PV system) and scarce predictable loads (EV charging and residential loads), the EMS allowed the VPP to be managed as a controllable unit, with small energy imbalances (on average, 148.69 kWh/day, i.e., 8% of the VPP daily energy requirement) and perfect reliability during the AS supply (no imbalances were detected during the service provision).

The results were achieved with a limited increase in the problem computational burden. Indeed, the time required to carry out the real-time dispatch considering the short-term uncertainties (16 s per time step in *RH Stc 7*) was only 12 s higher compared with that required with the deterministic approach (4 s per time step in *RH Det*). Hence, despite the greater model complexity, the proposed rolling horizon stochastic programming model is suitable for a real case study application.

In conclusion, the numerical evaluations confirmed that, in the presence of intermittent and non-programmable energy resources, the adoption of suitable models capable of handling the uncertainties affecting different time scales is pivotal.

In future studies, the effects of the market price uncertainties are an aspect requiring further evaluation. This could be carried out by extending the proposed scenarios generation method to also consider the correlation between market prices and RES production. Moreover, with a view to limiting the impacts of the DER dispatch on the underlying distribution network, the electrical grid model and the corresponding technical constraints could be included in the formulation. Although different studies can already be found in the literature including such technical constraints in their formulations, the computational times are usually significantly higher. Hence, techniques based on stochastic programming decomposition should be implemented.

CRediT authorship contribution statement

F. Gulotta: Conceptualization, Methodology, Software, Validation, Data curation, Visualization, Writing – original draft. **P. Crespo del Granado:** Conceptualization, Methodology, Resources, Writing – review & editing. **P. Pisciella:** Conceptualization, Methodology, Resources, Writing – review & editing. **D. Siface:** Conceptualization, Methodology, Validation, Supervision, Writing – review & editing. **D. Falabretti:** Conceptualization, Methodology, Validation, Writing – original draft, Supervision, Writing – review & editing, Project administration.

Declaration of Competing Interest

The authors declare that they have no known competing financial interests or personal relationships that could have appeared to influence the work reported in this paper.

Data availability

Data will be made available on request.

Acknowledgements

F. Gulotta PhD position and this research activity have been funded by Research Fund for the Italian Electric System in compliance with the Decree of the Italian Minister of Economic Development of April 16, 2018.

The authors acknowledge the Next generation Virtual Power Plant project co-financed by the Research Council of Norway (Grant 331720) under the Energy-X program.

References

[1] International Energy Agency (IEA). Net Zero by 2050: A Roadmap for the Global Energy Sector; 2021, available online: https://www.iea.org/reports/net-zero-by-2050.
[2] Baringo L, Rahimiyan M. Virtual power plants and electricity markets: decision making under uncertainty. Springer Nature Switzerland AG 2020. https://doi.org/10.1007/978-3-030-47602-1.
[3] Yu S, Fang F, Liu Y, Liu J. Uncertainties of virtual power plant: Problems and countermeasures. Appl Energy, Volume 239; 2019, doi: doi.org/10.1016/j.apenergy.2019.01.224.
[4] Fateh D, Eldoromi M, Birjandi AAM. 9 - Uncertainty modeling of renewable energy sources. Scheduling and Operation of Virtual Power Plants, Elsevier 2022:193–208. https://doi.org/10.1016/B978-0-32-385267-8.00014-7.
[5] Falabretti D, Gulotta F, Siface D. Scheduling and operation of RES-based virtual power plants with e-mobility: A novel integrated stochastic model. Int J Electr Power Energy Syst 2023;144. https://doi.org/10.1016/j.ijepes.2022.108604.
[6] Kochupurackal A, Pancholi KP, Islam SN, et al. Rolling horizon optimisation based peer-to-peer energy trading under real-time variations in demand and generation. Energy Syst 2022. https://doi.org/10.1007/s12667-022-00511-w.
[7] Vahedipour-Dahraie M, Rashidizadeh-Kermani H, Shafie-Khah M, Catalão JPS. Risk-averse optimal energy and reserve scheduling for virtual power plants incorporating demand response programs. IEEE Trans Smart Grid March 2021;12(2):1405–15. https://doi.org/10.1109/TSG.2020.3026971.
[8] Baringo L, Freire M, García-Bertrand R, Rahimiyan M. Offering strategy of a price-maker virtual power plant in energy and reserve markets. Sustain Energy Grids Networks 2021;28. https://doi.org/10.1016/j.segan.2021.100558.
[9] Baringo A, Baringo L, Arroyo JM. Day-ahead self-scheduling of a virtual power plant in energy and reserve electricity markets under uncertainty. IEEE Trans Power Syst May 2019;34(3):1881–94. https://doi.org/10.1109/TPWRS.2018.2883753.
[10] Oladimeji O, Ortega Á, Sigrist L, Rouco L, Sánchez-Martín P, Lobato E. Optimal Participation of Heterogeneous, RES-Based Virtual Power Plants in Energy Markets. Energies Apr. 2022;15(9):3207. https://doi.org/10.3390/en15093207.
[11] Nguyen HT, Le LB, Wang Z. A bidding strategy for virtual power plants with the intraday demand response exchange market using the stochastic programming. In: IEEE Transactions on Industry Applications, vol. 54, no. 4, pp. 3044-3055, July-Aug. 2018, doi: 10.1109/TIA.2018.2828379.
[12] Heitsch H, Römisch W. Scenario Reduction Algorithms in Stochastic Programming. Computational Optimization and Applications 24, 187–206 (2003). 5Thttps://doi.org/10.1023/A:102180592415257.
[13] Zhao Q, Shen Y, Li M. Control and bidding strategy for virtual power plants with renewable generation and inelastic demand in electricity markets. IEEE Trans Sustainable Energy April 2016;7(2):562–75. https://doi.org/10.1109/TSTE.2015.2504561.
[14] Shafiekhani M, Badri A, Shafie-khah M, Catalão JPS. Strategic bidding of virtual power plant in energy markets: A bi-level multi-objective approach. Int J Electr Power Energy Syst 2019;113. https://doi.org/10.1016/j.ijepes.2019.05.023.
[15] Ghorbankhani E, Badri A. A bi-level stochastic framework for VPP decision making in a joint market considering a novel demand response scheme. Int Trans Electr Energy Syst 2017;28. https://doi.org/10.1002/etep.2473.
[16] Rahimiyan M, Baringo L. Strategic bidding for a virtual power plant in the day-ahead and real-time markets: a price-taker robust optimization approach. IEEE Trans Power Syst July 2016;31(4):2676–87. https://doi.org/10.1109/TPWRS.2015.2483781.
[17] Cholette PA, Lamy R. Mutivariate ARIMA forecasting of irregular time series. Int J Forecasting, Volume 2, Issue 2, 1986, Pages 201-216, doi:10.1016/0169-2070(86)99004-7.
[18] Hadayeghparast S, Soltani A, Nejad Farsangi, Shayanfar H. Day-ahead stochastic multi-objective economic/emission operational scheduling of a large scale virtual power plant. Energy, Volume 172; 2019, doi: 10.1016/j.energy.2019.01.143.
[19] Shotorbani AM, Zeinal-Kheiri S, Chhipi-Shrestha G, Mohammadi-Ivatloo B, Sadiq R, Hewage K. Enhanced real-time scheduling algorithm for energy management in a renewable-integrated microgrid. Appl Energy 2021;304. https://doi.org/10.1016/j.apenergy.2021.117658.
[20] Akter MN, Mahmud MA, Haque ME, Amanullah M.T. Oo, An optimal distributed energy management scheme for solving transactive energy sharing problems in

residential microgrid. Appl Energy, Volume 270; 2020, doi: 10.1016/j.apenergy.2020.115133.
[21] Feng S, Yang D, Zhou B, Luo Y, Li G. Real-time active power dispatch of virtual power plant based on distributed model predictive control. Electron Lett 2022;58. https://doi.org/10.1049/ell2.12640.
[22] ENTSO-E. Market report 2021. available online: 5Thttps://www.entsoe.eu/news/2021/07/19/entso-e-releases-two-2021-market-monitoring-reports/5T, Date accessed June 22, 2022.
[23] Gulotta F. et al., Opening of the Italian Ancillary Service Market to Distributed Energy Resources: Preliminary Results of UVAM project. 2020 IEEE 17th International Conference on Smart Communities: Improving Quality of Life Using ICT, IoT and AI (HONET), 2020, pp. 199-203, doi: 10.1109/HONET50430.2020.9322822.
[24] Cobos NG, Arroyo JM, Alguacil N, Wang J. Robust energy and reserve scheduling considering bulk energy storage units and wind uncertainty. IEEE Trans Power Syst Sep. 2018;33(5):5206–16.
[25] Kim S, Rasouli S, Timmermans HJP, Yang D. A scenario-based stochastic programming approach for the public charging station location problem. Transportmetrica B: Transport Dynamics 2022;10(1):340–67. https://doi.org/10.1080/21680566.2021.1997672.
[26] Shapiro A, Philpott A. A Tutorial on Stochastic Programming; 2007, Manuscript available at 5Thttps://www.stoprog.org/sites/default/files/SPTutorial/TutorialSP.pdf5T.
[27] Andrenacci N, Vellucci F, Sglavo V. The Battery Life Estimation of a Battery under Different Stress Conditions. Batteries; 2021, 7, 88. 5Thttps://doi.org/10.3390/batteries70400885T.
[28] Conte F, Crosa di Vergagnia M, Massucco S, Silvestro F, Ciapessoni E, Cirio D. Performance analysis of frequency regulation services provided by aggregates of domestic thermostatically controlled loads. Int J Electr Power Energy Syst October 2021;131. https://doi.org/10.1016/j.ijepes.2021.107050.
[29] Belotti P, Bonami P, Fischetti M. et al. On handling indicator constraints in mixed integer programming. Comput Optim Appl 65, 545–566 (2016). 5Thttps://doi.org/10.1007/s10589-016-9847-85T.
[30] Clò S, Fumagalli E. The effect of price regulation on energy imbalances: A Difference in Differences design. Energy Econ June 2019;81:754–64. https://doi.org/10.1016/j.eneco.2019.05.008.
[31] Chen C, Wang J, Heo Y, Kishore S. MPC-based appliance scheduling for residential building energy management controller. IEEE Trans Smart Grid Sept. 2013;4(3):1401–10. https://doi.org/10.1109/TSG.2013.2265239.
[32] Julia L. Higle. Stochastic Programming: Optimization When Uncertainty Matters. INFORMS TutORials in Operations Research: 30-53, doi: 10.1287/educ.1053.0016.
[33] Italian Energy Services Operator (GSE), "Photovoltaic Statistical report", 2021, available online: https://www.gse.it/documenti_site/Documenti%20GSE/Rapporti%20statistici/Solare%20Fotovoltaico%20-%20Rapporto%20Statistico%202021.pdf.
[34] Pellegrino L, Sandroni C. Aggregation of residential Energy Storage Systems. AEIT International Annual Conference (AEIT) 2019;2019:1–6. https://doi.org/10.23919/AEIT.2019.8893288.
[35] Conte F, Gabriele B, Massucco S, Silvestro F, Cirio D, Croci L. Flexibility Evaluation of Domestic Electric Water Heater Aggregates. IEEE Madrid PowerTech 2021;2021:1–6. https://doi.org/10.1109/PowerTech46648.2021.9494972.
[36] Falabretti D, Gulotta F, Siface D. Residential Users as Flexibility Providers: a Techno-Economic Analysis. In: 2022 18th International Conference on the European Energy Market (EEM), 2022, pp. 1-6, doi: 10.1109/EEM54602.2022.9921077.
[37] Benetti G, Delfanti M, Facchinetti T, Falabretti D, Merlo M. Real-time modeling and control of electric vehicles charging processes. IEEE Trans Smart Grid May 2015;6(3):1375–85. https://doi.org/10.1109/TSG.2014.2376573.
[38] Automobile Club d'Italia (ACI), Dati e statistiche, Available online: http://www.aci.it/laci/studie-ricerche/dati-e-statistiche.html.
[39] Italian Electricity Market Operator website, data available online: 5Thttps://www.mercatoelettrico.org/It/Esiti/MSD/MSDex-ante.aspx5T.
[40] Falabretti D, Gulotta F. A Nature-Inspired Algorithm to Enable the E-Mobility Participation in the Ancillary Service Market. Energies 2022;15, 3023. https://doi.org/10.3390/en15093023.
[41] Adhikari R, Agrawal RK. An Introductory Study on Time Series Modeling and Forecasting, [Online]. Available: 5Thttps://arxiv.org/abs/1302.66135T.
[42] Akaike H. A new look at the statistical model identification. IEEE Trans Autom Control December 1974;19(6):716–23. https://doi.org/10.1109/TAC.1974.1100705.
[43] Leonard Kaufman, Peter J. Rousseeuw. Finding Groups in Data: An Introduction to Cluster Analysis. 10.1002/9780470316801.
[44] Rousseeuw Peter J. Silhouettes: A graphical aid to the interpretation and validation of cluster analysis. J Comput Appl Math 1987;20. https://doi.org/10.1016/0377-0427(87)90125-7.
[45] Chodakowska E, Nazarko J, Nazarko Ł. ARIMA models in electrical load forecasting and their robustness to noise. Energies Nov. 2021;14(23):7952. https://doi.org/10.3390/en14237952.
[46] Huang S-J, Shih K-R. Short-term load forecasting via ARMA model identification including non-Gaussian process considerations. IEEE Trans Power Syst May 2003;18(2):673–9. https://doi.org/10.1109/TPWRS.2003.811010.
[47] Holan SH, Lund R, Davis Ginger. The ARMA alphabet soup: A tour of ARMA model variants. Statist Surv 2010;4:232–74. https://doi.org/10.1214/09-SS060.
[48] Singh B, Pozo D. A Guide to Solar Power Forecasting using ARMA Models. In: 2019 IEEE PES Innovative Smart Grid Technologies Europe (ISGT-Europe); 2019, pp. 1-4, doi: 10.1109/ISGTEurope.2019.8905430.
[49] Wynn SLL, Boonraksa T, Boonraksa P, Pinthurat W, Marungsri B. Decentralized energy management system in microgrid considering uncertainty and demand response. Electronics Jan. 2023;12(1):237. https://doi.org/10.3390/electronics12010237.
[50] David M, Ramahatana F, Trombe PJ, Lauret P. Probabilistic forecasting of the solar irradiance with recursive ARMA and GARCH models. Solar Energy, Volume 133, 016, doi: 10.1016/j.solener.2016.03.064.
[51] Kębłowski P, Welfe A. The ADF–KPSS test of the joint confirmation hypothesis of unit autoregressive root. Economics Letters, Volume 85, Issue 2, doi: 10.1016/j.econlet.2004.04.013.
[52] Smith TG. "pmdarima", available online: https://github.com/alkaline-ml/pmdarima.
[53] Pilo F. et al., Impact of Electrical Vehicle Residential Charging Stations on the Quality of the Low Voltage Network Supply. 2022 20th International Conference on Harmonics & Quality of Power (ICHQP), 2022, pp. 1-6, doi: 10.1109/ICHQP53011.2022.9808715.
[54] Chen Y, Fuchs H, Schein J, Franco V, Stratton H, Dunham C. Calculating average hot water mixes of residential plumbing fittings. available online: US Environmental Protection Agency report 2020. 5Thttps://escholarship.org/uc/item/9m90p3qh5T.
[55] Haggi H, Sun W, Fenton JM, Brooker P. Proactive Rolling-Horizon-Based Scheduling of Hydrogen Systems for Resilient Power Grids. IEEE Trans Ind Appl March-April 2022,;58(2):1737–46. https://doi.org/10.1109/TIA.2022.3146848.
[56] Hart W, Watson JP, Woodruff DL. Pyomo: modeling and solving mathematical programs in Python. Math Program Comput 2011;3. https://doi.org/10.1007/s12532-011-0026-8.